REPORT DOCUMENTATION PAGE

1a. REPORT SECURITY CLASSIFICATION: UNCLASSIFIED	1b. RESTRICTIVE MARKINGS
2a. SECURITY CLASSIFICATION AUTHORITY	3 DISTRIBUTION / AVAILABILITY OF REPORT: Approved for public release; distribution is unlimited
2b. DECLASSIFICATION / DOWNGRADING SCHEDULE	
4. PERFORMING ORGANIZATION REPORT NUMBER(S)	5. MONITORING ORGANIZATION REPORT NUMBER(S): CR 89-02
6a. NAME OF PERFORMING ORGANIZATION: Dept. of Atmospheric Sciences, University of Washington; 6b. OFFICE SYMBOL (If applicable)	7a. NAME OF MONITORING ORGANIZATION: Naval Environmental Prediction Research Facility
6c. ADDRESS (City, State, and ZIP Code): Seattle, WA 98195	7b. ADDRESS (City, State, and ZIP Code): Monterey, CA 93943-5006
8a. NAME OF FUNDING / SPONSORING ORGANIZATION: Office of Naval Research; 8b. OFFICE SYMBOL (If applicable): ONT	9. PROCUREMENT INSTRUMENT IDENTIFICATION NUMBER: N00014-86-K-0453
8c. ADDRESS (City, State, and ZIP Code): Arlington, VA 22217	10 SOURCE OF FUNDING NUMBERS

PROGRAM ELEMENT NO.	PROJECT NO.	TASK NO.	WORK UNIT ACCESSION NO.
62435N	R3582		DN656759

11. TITLE (Include Security Classification): Application of Special Sensor Microwave/Imager Data for Analysis of Cyclonic Storms in Midlatitudes over the Sea (U)

12. PERSONAL AUTHOR(S): Katsaros, Kristina B.; Petty, Grant W.; Bhatti, Iftekhar; and Miller, Douglas

13a. TYPE OF REPORT	13b. TIME COVERED	14. DATE OF REPORT (Year, Month, Day)	15. PAGE COUNT
Annual	FROM 8/87 TO 11/88	1989, March	40

16. SUPPLEMENTARY NOTATION

17 COSATI CODES			18. SUBJECT TERMS (Continue on reverse if necessary and identify by block number)
FIELD	GROUP	SUB-GROUP	Satellite, Microwave, Fronts, Precipitation, Precipitable water
04	01		

19. ABSTRACT (Continue on reverse if necessary and identify by block number)

In the first contract year of this work we developed algorithms and criteria for identifying fronts in cyclonic weather systems with data on atmospheric water vapor and rain obtained with microwave sensors in space. Using data from the 18, 21 and 37 GHz channels of the Scanning Multichannel Microwave Radiometer (SMMR) on the SEASAT and NIMBUS-7 satellites, we calculated fields of these variables in cyclonic storms.

This report covers work performed in the second year and is concerned with the currently operating microwave radiometer, the Special Sensor Microwave/Imager (SSM/I) on the F8 satellite in the Defense Meteorological Satellite Program (DMSP). This sensor employs three frequencies with similar characteristics as the ones giving atmospheric water data on SMMR, but not at exactly the same frequencies. For this reason we needed to test the algorithms for identifying fronts with data from this new sensor. In addition, the SSM/I has two channels at 85 GHz which are sensitive to scattering caused by large ice

((continued on reverse))

20. DISTRIBUTION / AVAILABILITY OF ABSTRACT: ☒ UNCLASSIFIED/UNLIMITED ☐ SAME AS RPT ☐ DTIC USERS	21. ABSTRACT SECURITY CLASSIFICATION: UNCLASSIFIED
22a NAME OF RESPONSIBLE INDIVIDUAL: Dr. Paul M. Tag, contract monitor	22b. TELEPHONE (Include Area Code): (408) 647-4737; 22c. OFFICE SYMBOL: NEPRF WU 6.2-9

Block 19, Abstract, continued

particles and graupel in the clouds. We found that an index of this scattering gives a unique view of the deep clouds in frontal zones. We also tested cloud liquid water and wind algorithms developed for SSM/I, and found good qualitative agreement with conventional data.

Several cyclones occurring in the fall of 1987 were examined in some detail. It is clear that microwave sensing of these weather systems from space can give the analyst unique and very useful information to better locate fronts, convective regions, and other weather phenomena over the oceans.

AN (1) AD-A207 675
FG (2) 040100
CI (3) (U)
CA (5) NAVAL ENVIRONMENTAL PREDICTION RESEARCH FACILITY MONTEREY CA
TI (6) Application of Special Sensor Microwave/Imager Data for Analysis of Cyclonic Storms in Midlatitudes Over the Sea.
TC (8) (U)
DN (9) Annual rept. Aug 87-Nov 88,
AU (10) Katsaros, Kristina B.
AU (10) Petty, Grant W.
AU (10) Bhatti, Iftekhar
AU (10) Miller, Douglas
RD (11) Mar 1989
PG (12) 42
CT (15) N00014-86-K-0453
PJ (16) R3582
RN (18) NEPRF-R-89-02
RC (20) Unclassified report
DE (23) *ATMOSPHERIC PRECIPITATION, *CYCLONES, *FRONTS, (METEOROLOGY), *RADIOMETERS, *ELECTROMAGNETIC SCATTERING, ALGORITHMS, CLOUDS, CONVECTION(ATMOSPHERIC), DEPARTMENT OF DEFENSE, DETECTION, DETECTORS, DUAL CHANNEL, EARTH ATMOSPHERE, FREQUENCY, HYDROMETEORS, ICE, IMAGES, LIQUIDS, MARINE METEOROLOGY, METEOROLOGICAL SATELLITES, MICROWAVE EQUIPMENT, MICROWAVE FREQUENCY, MULTICHANNEL, OCEANS, PARTICLES, RAIN, REGIONS, SCANNING, SENSITIVITY, SPACEBORNE, STORMS, WATER, WATER VAPOR, WEATHER, WIND.
DC (24) (U)
ID (25) Liquid water, Microwave detectors, Midlatitudes, SMMR(Scanning Multichannel Microwave Radiometers), PE62435N, WUDN6S6759.
IC (26) (U)
AB (27) Previously we developed algorithms and criteria for identifying fronts in cyclonic weather systems with data on atmosoneric water vapor and rain obtained with microwave sensors in space. Using data from the 18, 21 and 37 GHz channels of the Scanning Multichannel Microwave Radiometer (SMMR) on the SEASAT and NIMBUS-7 satellites, we calculated fields of these variables in cyclonic storms. This report is concerned with currently operating microwave radiometer, the Special Sensor Microwave/Imager (SSM/I) on the F8 satellite in the Defense Meteorological Satellite Program (DMSP). This sensor employs three frequencies with similar characteristics as the ones giving atmospheric water data on SMMR, but not at exactly the same frequencies. For this reason we needed to test the algorithms for identifying fronts with data from this new sensor. In addition, the SSM/I has two channels at 85 GHz which

are sensitive to scattering caused by large ice particles and graupel in the clouds. We found that an index of this scattering gives a unique view of the deep clouds in frontal zones. We also tested cloud liquid water and wind algorithms developed for SSM/I, and found good qualitative agreement with conventional

data. Several cyclones occuring in the fall of 1987 were examined in some detail. It is clear that microwave sensing of these weather systems from space can give the analyst unique and very useful information to better locate fronts, convective regions, and other weather phenomena over the oceans. Keywords: Meteorological fronts; Atmospheric precipitation; Precipitable water. (eac)
AC (28) (U)
DL (33) 01
SE (34) A
CC (35) 407279

Naval Environmental Prediction Research Facility
Monterey, CA 93943-5006
Contractor Report CR 89-02 March 1989

APPLICATION OF SPECIAL SENSOR MICROWAVE/IMAGER DATA FOR ANALYSIS OF CYCLONIC STORMS IN MIDLATITUDES OVER THE SEA

by Kristina B. Katsaros, Grant W. Petty, Iftekhar Bhatti, Douglas Miller
University of Washington Seattle, WA 98195

CONTENTS

1. INTRODUCTION

During the first year of this project our main objective was to establish the statistical validity of locating atmospheric fronts by flagging strong gradients in integrated atmospheric water vapor (IWV) and rain occurrence obtained by analyzing data from the Scanning Multichannel Microwave Radiometer (SMMR) on the Nimbus 7 and Seasat satellites. Sixty-five cases of swaths over the oceans in both hemispheres were studied and the limiting values for the gradient in IWV and the value of the 37 GHz brightness temperature (related to rain occurrence) which locates fronts were established (Katsaros, et al., 1988a). An article has been produced for the Journal of Weather Forecasting (Katsaros, et al., 1988b) which has been conditionally accepted pending revisions. In the second year of this contract our objective was to make a preliminary investigation of how the experience with SMMR data translates to data from the operational Special Sensor Microwave/Imager (SSM/I). This instrument is on the Defense Meteorological Satellite Program (DMSP) F8 satellite launched in June, 1987. Its three lowest frequencies correspond to the three higher ones of SMMR, which are the ones employed for the work covered in our First Annual Report (Table I).

This year's report is more limited in scope than the first year's. The First Annual Report covered work performed over a 15-month period, since at the end of that time we had reached a natural break point, having finished the work with SMMR data. In the remaining 9 months of the second year we have acquired SSM/I tapes from E. Francis and F.J. Wentz* by duplicating their compact format tapes here at the University of Washington , and have applied the algorithms delivered by the Hughes Aircraft Co. with the SSM/I

---

* Remote Sensing Systems, Inc., Santa Rosa, CA.

instrument (Hollinger, et al., 1987) to case studies of storms in the North Pacific and North Atlantic Oceans. We have looked mainly at integrated water vapor (IWV), integrated cloud liquid water (ICLW), rain occurrence and surface wind speed. Because of the recent launch of the DMSP F8 satellite, only data from the month of October 1987 were available to be included in this study. We have adapted our gradient and rain flag subroutines to the SSM/I, and have evaluated thresholds for this new sensor.

Table I. ***Characteristics of the Two Polar Orbiting Radiometers - SMMR on Seasat and on Nimbus 7 and the SSM/I on the F8 DMSP Satellite***

SMMR

FREQ. GHz	APPROX. RESOLUTION (km)
6.6	150
10.7	100
18	65
21	60
37	35
--	--

Swath Width:
Seasat: 650 km
Nimbus 7: 780 km

Period of Operation:
Seasat: July-October 1978
Nimbus 7: October 1978-Fall, 1987

SSM/I

FREQ. GHz	APPROX. RESOLUTION (km)
--	--
--	--
19.35	55
22.235	50
37	35
85.5	15

Swath Width: 1400 km

Period of Operation:
July, 1987 - Present

In Section 2 we describe the procedures and the algorithms used, and the necessary modifications to our previous flagging routine that is now based on SSM/I data. In Section 3 we present our results by taking the reader through several case studies. In Section 4 we discuss the implications of our work for future use of SSM/I data.

2. ANALYSIS PROCEDURES

2.1 Data Source

SSM/I antenna temperatures were obtained in the form of compact-format 6250 BPI digital tapes from Remote Sensing Systems, Inc. These tapes each contain four full days of global SSM/I data. Computer subroutines were provided with the tapes to unpack logical data records and to convert antenna temperatures to brightness temperatures (Tb's). A report by Wentz and Francis describing both the contents of the tapes and the accompanying decoding procedures will appear in early 1989.

Some hardware-related difficulties were initially experienced in reading and copying the data tapes, apparently due to the large physical record size of these tapes. Although we were able to improvise a temporary "fix" for this problem, a satisfactory permanent solution is still being sought, with the cooperation of both the system administrator of the department's Prime minicomputer and the computer's manufacturer.

A major component of our efforts to work with the new SSM/I data has been the development of local software packages for interactive screening, display, analysis, and the plotting of various SSM/I derived parameters. This project is nearing completion and has reached the stage where these data can now be quickly and efficiently searched and processed. The cases discussed in this report represent some of the first results.

2.2 Algorithms

The SSM/I was delivered to the U.S. Navy from the Hughes Aircraft Company with a set of algorithms for calculating various parameters (Hollinger, et al., 1987). Since our task was to evaluate the performance of the system, we employed these algorithms, even though predictions had already been made that improvements would be needed (Wentz, et al., 1986). This prediction is not surprising since a long time had passed between the design of

the sensor and its algorithms in the late 1970's to the launch in 1987. A better algorithm has been proposed (Wentz, et al., 1986), particularly for wind speed. At the University of Washington we are also developing new algorithms for ocean surface parameters (sea surface temperature and wind speed) and for the atmospheric water parameters, integrated water vapor (IWV), integrated cloud liquid water (ICLW) and rain rate (G.W. Petty, Ph.D. thesis work). Since these algorithms are still under development, we have used mainly the Hughes algorithms for this work, but a few examples of storm analyses that depend on some use of the experimental algorithms are included.

The following parameters are calculated using the Hughes algorithms, which consist of linear combinations of brightness temperatures from up to four SSM/I channels. The channels used, and their season- and climate-dependent coefficients, are given by Hollinger, et al.(1987).

Integrated Water Vapor (IWV): Preliminary evaluations by other investigators (e.g., Alishouse, personal communication, 1988) suggest that this parameter is retrieved quite reliably by the SSM/I in midlatitude zones, with errors of less than 10%.

Integrated Cloud Liquid Water (ICLW): Qualitative patterns generally look reasonable, but the frequent appearance of negative values suggests a bias in the retrieved values. *In situ* verification of SSM/I cloud water retrievals over the ocean has not yet been reported.

Wind Speed: Early experience with this parameter suggests the possible presence of a positive bias of order 5 m/sec. Further verification is necessary. Errors become large in the presence of rain and large cloud liquid water content.

The remaining parameters are obtained using experimental, in-house algorithms:

Rain Occurrence: Brightness temperature for the 37 GHz, horizontal polarization channel of the SSM/I increases dramatically in the presence of rain over the ocean. A threshold of 200 K appears to be a reliable indicator of rain occurrence. This value is slightly larger than the 190 K threshold used with SMMR data in our previous report, attributable to the greater incidence angle of the SSM/I. The incidence angle, i.e., angle between the local vertical and the direction to the satellite instrument, was 50° for the Nimbus 7 SMMR and is 53° for the SSM/I. Greater incidence angle results in a longer path through the rain.

Scattering by large ice particles: The short wavelength of the 85 GHz channels make them sensitive to scattering by precipitation-size ice particles. These particles appear to be associated primarily with regions of enhanced vertical motion and precipitation in midlatitude cyclones. The scattering signal is found by an index, S, which depends on the 85 GHz brightness temperatures in vertical (T_{85V}) and horizontal (T_{85H}) polarization:

$$S = -0.12\, T_{85V} + 0.064\, T_{85H} + 15.5$$

The physical motivation for scattering-based precipitation indices like the one above is outlined by Spencer (1986). In this report we have used data from the first four months of SSM/I operation. The T_{85V} channel developed gain problems some time into the mission (C. Crosiar, personal communication). We are not at present fully informed of the magnitude of the problem, or if corrections can be applied. Therefore, this channel should be used with caution.

Water vapor gradient flag: Scalar water vapor gradient is calculated for SSM/I water vapor fields as described for the SMMR in our first report. Due to the higher spatial sampling of the SSM/I, it was necessary to modify the smoothing procedure in order to obtain results comparable to those from the SMMR. Instead of a median filter with a 3 x 3 pixel window, as was used for the SMMR, a moving-average filter with a 5 x 5 pixel window was used. The larger window permits smoothing on a similar scale (approximately 150 km) as was used with the earlier sensor. The calculation of a mean instead of a median for the 25-pixel window has the advantage of being computationally much simpler and does not appear to substantially alter the results. In a further modification of the earlier SMMR gradient algorithm, geometric factors are used in calculating the gradient components in order to correct for the noncartesian geometry of the SSM/I data arrays.

In order to test WVG and rain occurrence flags, several threshold values were tried. For the water vapor gradient (WVG) values of 0.06, 0.10 and 0.12 kg m^{-2}/km were tried. The lowest value (0.06) corresponds approximately to the optimum threshold which we established in our earlier work with the SMMR. Figure 1a, b, c shows the fields of the WVG flag produced with these three different values of the threshold for one well developed frontal region. All values of the WVG greater than the threshold are flagged. The surface location of the fronts on Figures 1a, b, c have been advected from the position on the National Meteorological Center (NMC) analysis for 18 UTC. It appears that the value 0.10 kg m^{-2}/km outlines the frontal zone, but does not flag extraneous regions, except that occasionally the southernmost side of the pre-cold frontal maximum in IWV has as sharp a gradient as the postfrontal side, particularly far from the low pressure center near the tail of the cold front.

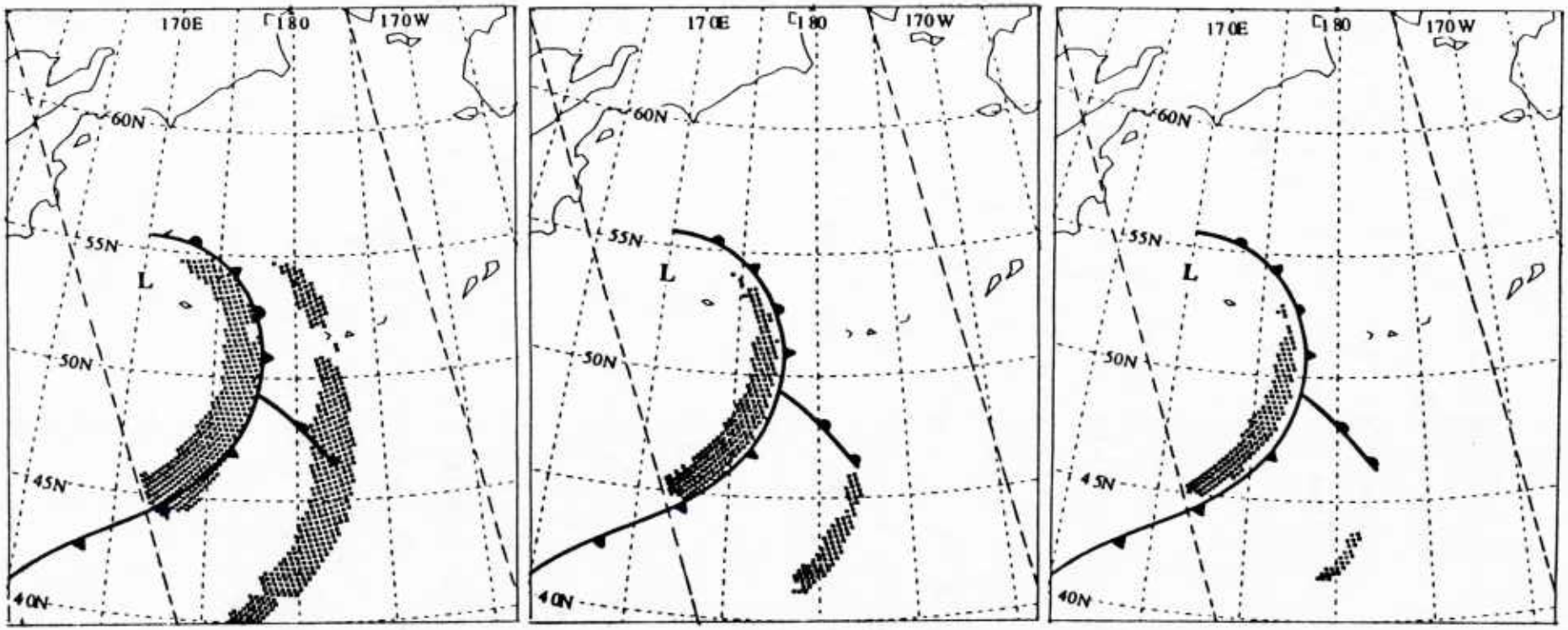

(a) Water vapor gradient flag '*' plotted for threshold values of (.06 kg m^{-2})/km.

(b) Water vapor gradient flag '*' plotted for threshold values of (.1 kg m^{-2})/km.

(c) Water vapor gradient flag '*' plotted for threshold values of (.12 kg m^{-2})/km.

Figure 1(a)-(c). The appearance of the water vapor gradient (WVG) flags for three threshold values: .06, .10 and .12 (kg m^{-2})/km for DMSP F8 SSM/I, October 30, 1987, 17:31 UTC, Orbit #1873 as it passed over an occluded cyclone in the North Pacific Ocean. The frontal analysis is our estimate of the frontal location based on the IWV data.

The rain occurrence flag was also tested for three values of the threshold: 190°, 200° and 205°K. For SMMR we had used a threshold of 190°K. Figure 2 shows the rain flag for the frontal system shown in Figure 1. The choice of a threshold value for SSM/I was made subjectively by inspection of several frontal zones and by comparison to the appearance of similar cases studied with SMMR data (Katsaros, et al., 1988a). In the cases presented below, a threshold of 200°K was used.

Before calculating wind speed with the Hughes algorithm we blocked out regions where calculated ICLW content was greater than zero, since the wind algorithm fails where ICLW dominates the emission. Because of the previously discussed negative bias in the ICLW estimates, our use of zero ICLW to screen out contaminated wind estimates is not nearly as conservative as it seems, but rather represents an unknown positive threshold of actual water content which seems, fortuitously, to reliably delineate problem areas in the estimated wind speed field.

3. RESULTS

3.1 Case Studies from the North Pacific Ocean.

October 25-26, 1987

A mature cyclone with low pressure center at 45°N, 168°W is seen in the surface analysis by the National Meteorological Center in Figure 3a with the associated GOES infrared image in Figure 3b. Figure 3c shows the IWV contours with the frontal position analyzed by NMC for a satellite pass close in time to this analysis. The two consecutive satellite passes of the region are seen in Figures 3d and e. Figure 3f shows the WVG flags for the three SSM/I swaths at 05:23 UTC on October 25, and at 05:07 and 14:58 UTC on October 26.

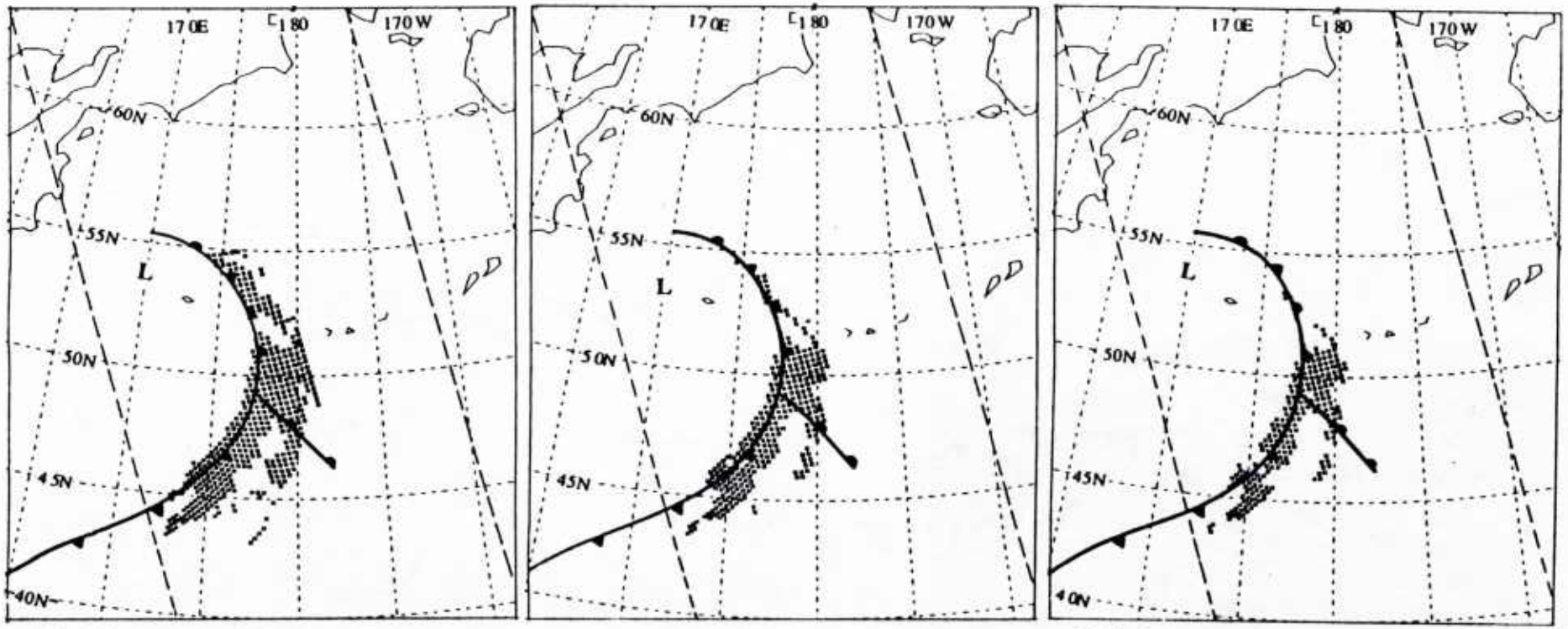

(a) Rain occurrence '*' based on a Tb_{37H} threshold of 190K.

(b) Rain occurrence '*' based on a Tb_{37H} threshold of 200K.

(c) Rain occurrence '*' based on a Tb_{37H} threshold of 205K.

Figure 2(a)-(c). The appearance of the rain occurrence flags for three threshold values of T37H: 190°K, 200°K and 205°K for data from DMSP F8 SSM/I, on October 30, 1987, 17:31 UTC, Orbit #1873. The frontal location is our best estimate.

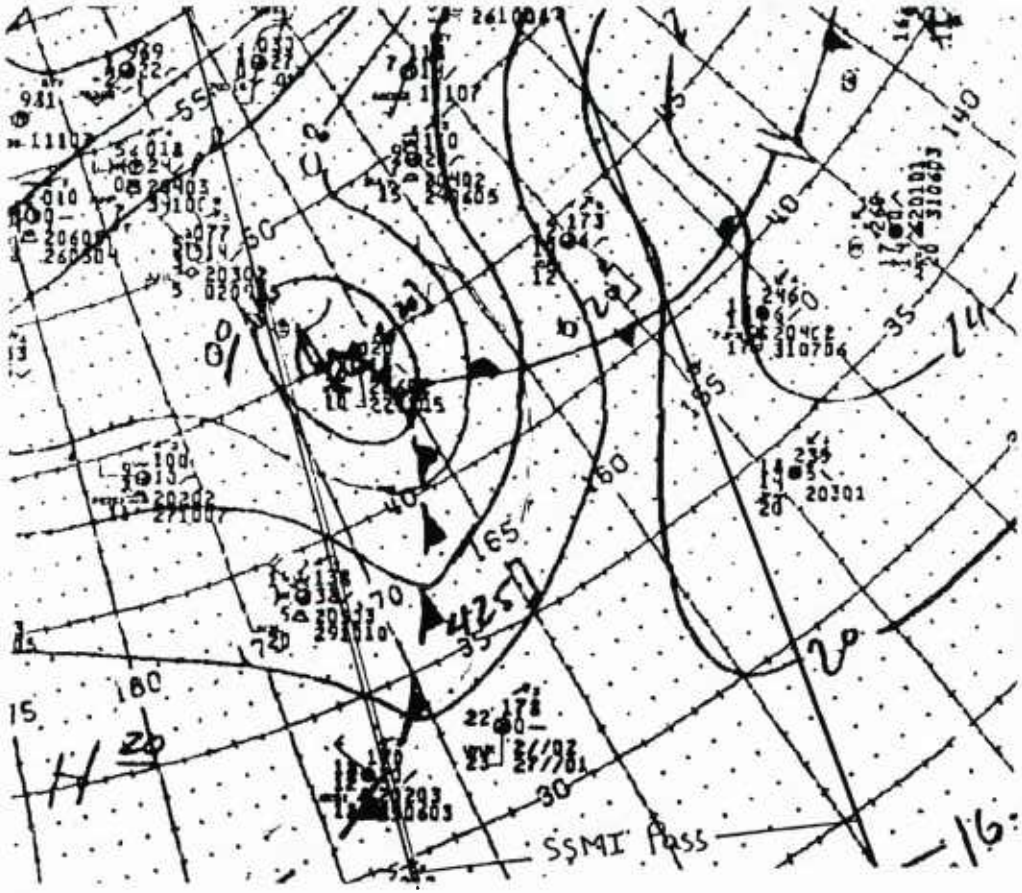

(a) NMC surface analysis, October 25, 06:00 UCT.

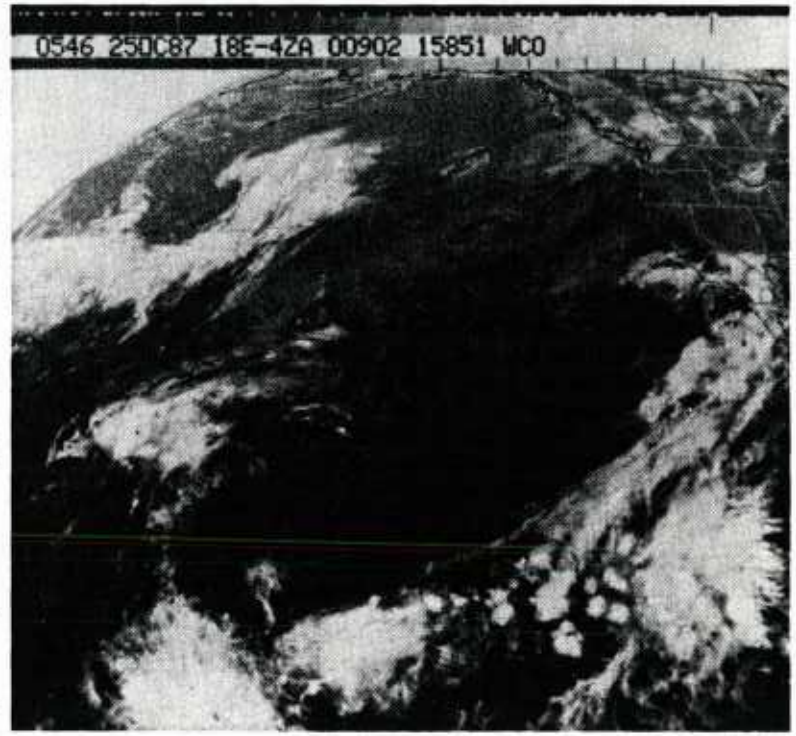

(b) GOES West infrared satellite image of the North Pacific Ocean for October 25, 05:46 UCT.

Figure 3(a)-(b). Frontal system crossing the Pacific Ocean, seen in operational data, October 25-26, 1987.

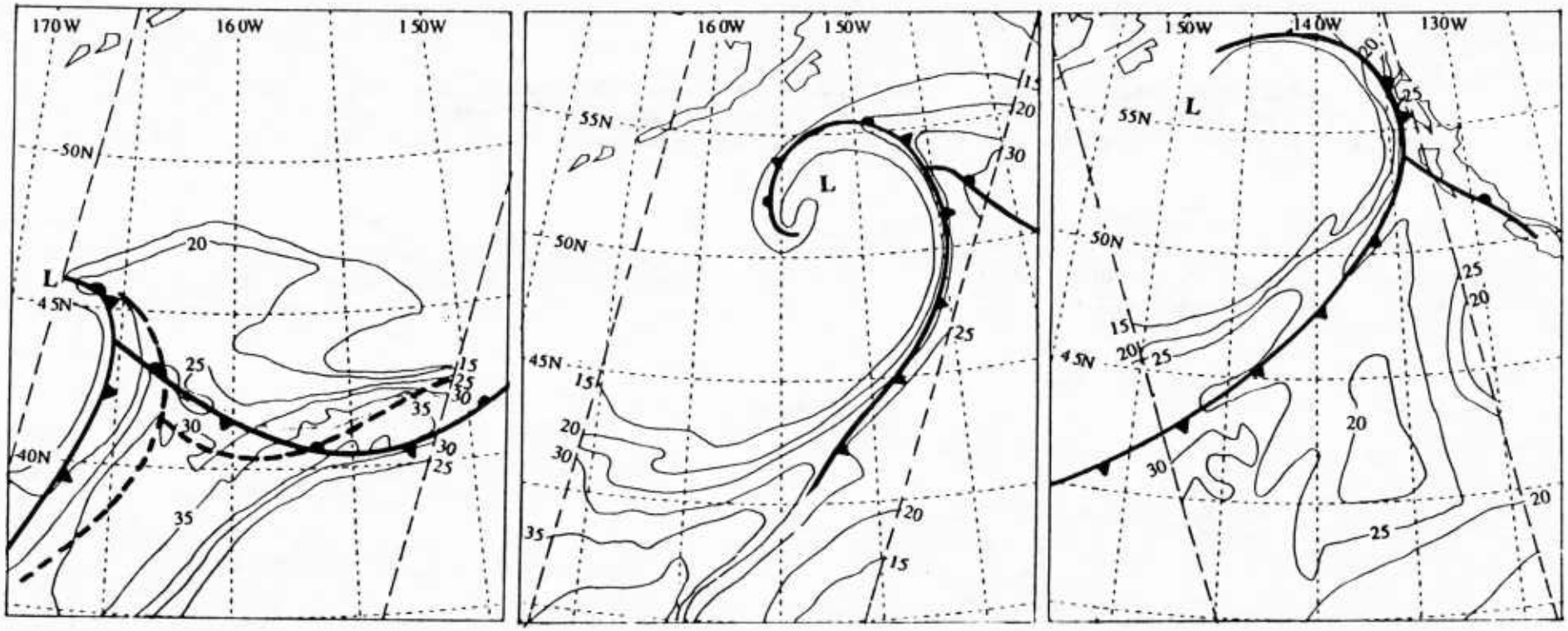

(c) Integrated water vapor values in kg m^{-2}, October 25, 05:23 UTC,Orbit #1795.

(d) Integrated water vapor values in kg m^{-2}. October 26, 05:07 UTC, Orbit #1809.

(e) Integrated water vapor values in kg m^{-2}. October 26, 14:58 UTC, #Orbit 1815.

Figure 3(c)-(e). Frontal system crossing the Pacific Ocean seen in DMSP F8 SSM/I data. Integrated Water Vapor for three consecutive passes. The superimposed frontal analyses are from NMC synoptic surface maps with the positions linearly interpolated to the times of the three orbits. The dashed frontal position in Figure (c) is our estimate of where it ought to be.

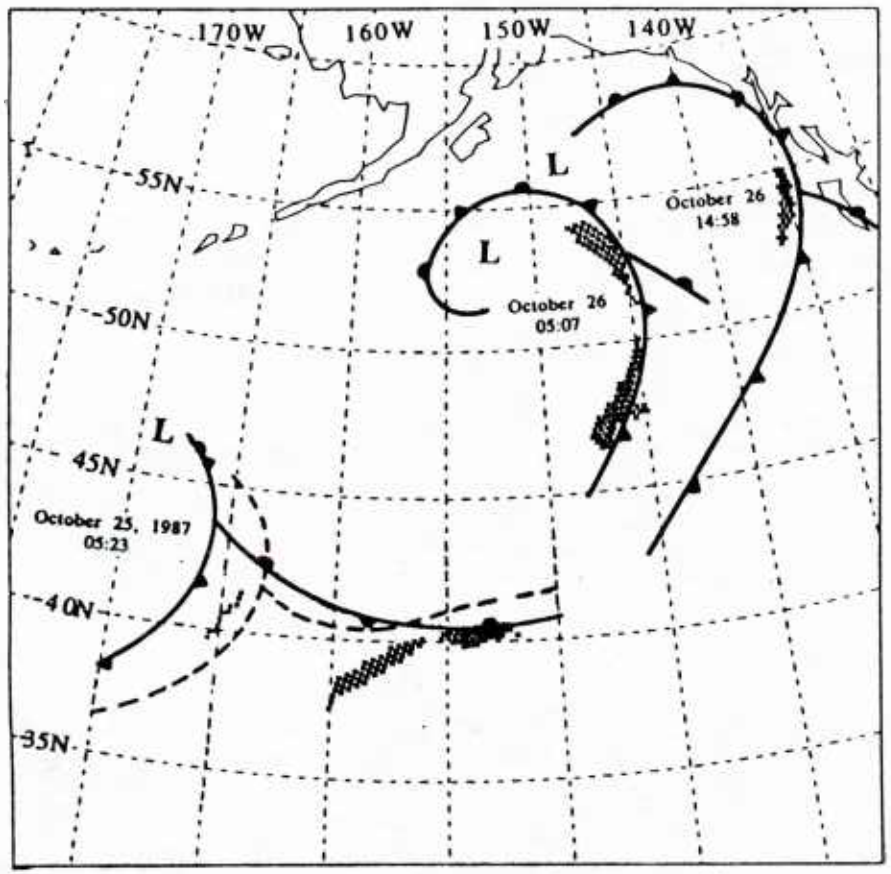

(f) Water vapor gradient flag '*' for all three orbits, plotted for threshold values of (.1 kg m^{-2})/km.

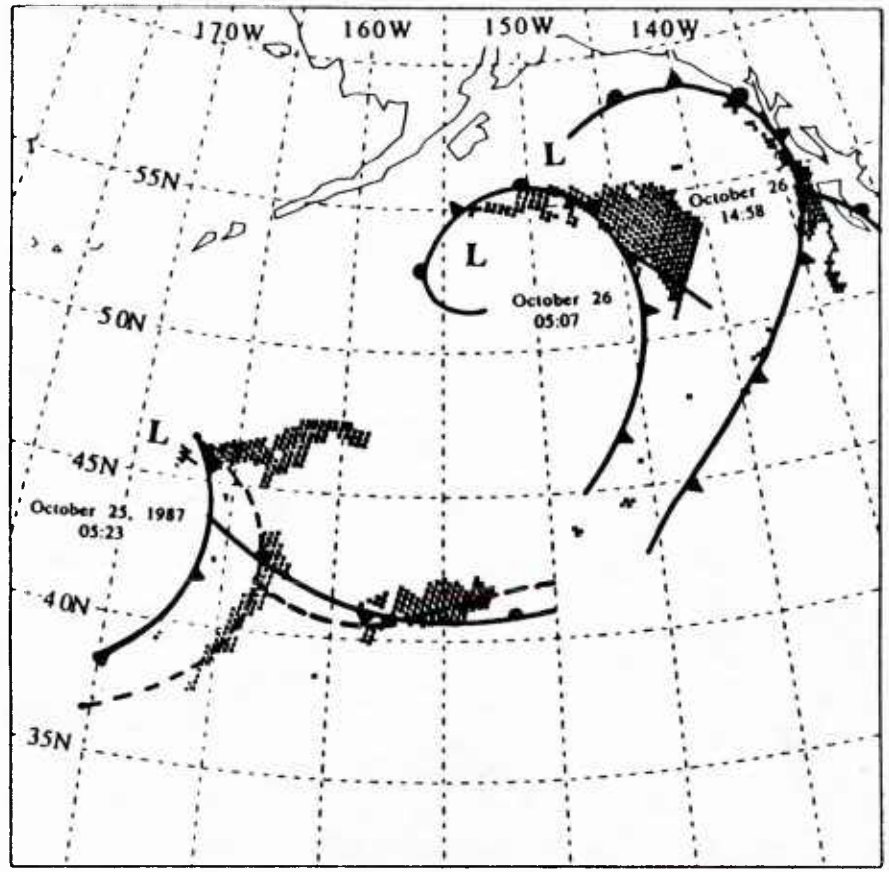

(g) Rain occurrence '*' for all three orbits, based on Tb37H threshold of 200K.

Figure 3(f)-(g). Integrated Water Vapor gradient flags and rain flags for the same three consecutive passes as in Figures 3 (c)-(e). The superimposed frontal analyses are from NMC synoptic surface maps with the positions linearly interpolated to the times of the three orbits. The dashed frontal position in the figures is our estimate of where it ought to be.

By our flagging criterion the NMC analysis in Figure 3c shows the cold front 2-3° of longitude too far westward. The positions of the front which we infer from the WVG are dashed in Figures 3c and f. This position is corroborated by the rain flag pattern in Figure 3g.

October 29-30, 1987

This case has been included to illustrate how well frontal zones are located with the WVG and rain flags, and how the improved sampling by SSM/I over SMMR allows one to follow the development and advance of weather systems as they cross the Pacific Ocean. Figures 4a, b, c show the contours of IWV for three orbits over a 22 hour period; note that swaths are not equally spaced in time. The superimposed frontal analyses are taken directly from the NMC analyses with interpolation to the time of the overpass. Figures 4d and e show the corresponding WVG and the rain flags for the three orbits. An adjustment of the position of the triple point between cold, warm and occluded fronts for 19:24 UTC on October 29, seems warranted based on the rain flag, the new position being at 50°N, 160°E. The new position is not in disagreement with the WVG-flags, since they do not outline this region of the frontal system at all. The new position of the triple point would be showing a more consistent movement of the frontal system with time. Otherwise, an unrealistic 15° longitude jump in position is implied between October 29, 19:24 UTC and October 30, 07:41 UTC. The frontal position at this latter time also appears to require a slight adjustment (this time, to the west), when looking at the WVG-flag, but the rain flag is in agreement with the NMC position. Inspection of the contours of IWV in Figure 4b reveals that probably the true frontal location is slightly *eastward* of the NMC analysis and that a slightly lower threshold for the WVG-flag would have flagged this region. However, if a lower threshold for WVG flags had been used it would also flag more of the opposite side of the maximum in IWV (a little line of WVG flags is seen at 43-45°N and 173°E, which belongs to the October 30, 07:41 UTC orbit).

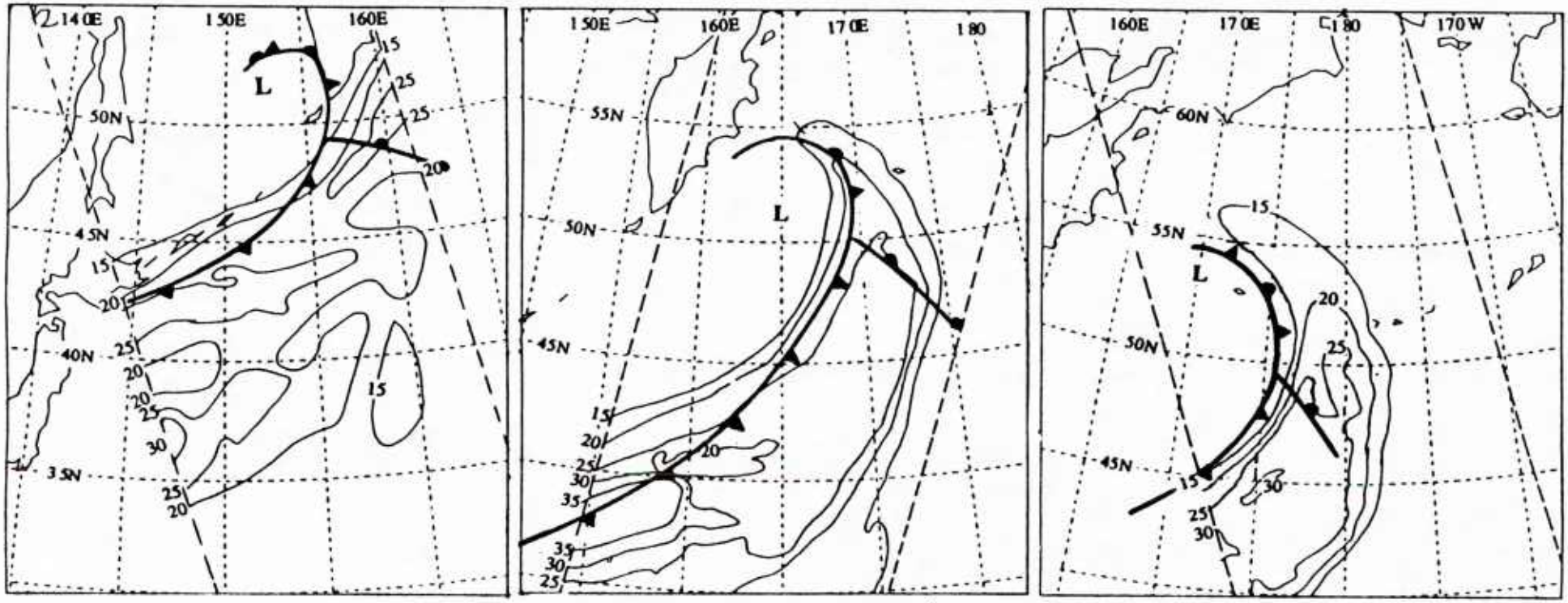

(a) Integrated water vapor values in kg m^{-2}, October 29, 19:24 UTC, Orbit #1860.

(b) Integrated water vapor values in kg m^{-2}, October 30, 07:41 UTC, Orbit #1867.

(c) Integrated water vapor values in kg m^{-2}, October 30, 17:31 UTC, Orbit #1873.

Figure 4(a)-(c). Occluded frontal systems crossing the Pacific Ocean, seen in DMSP F8 SSM/I data, October 29-30, 1987. The superimposed frontal analyses are from NMC synoptic surface maps with the positions linearly interpolated to the times of the three orbits.

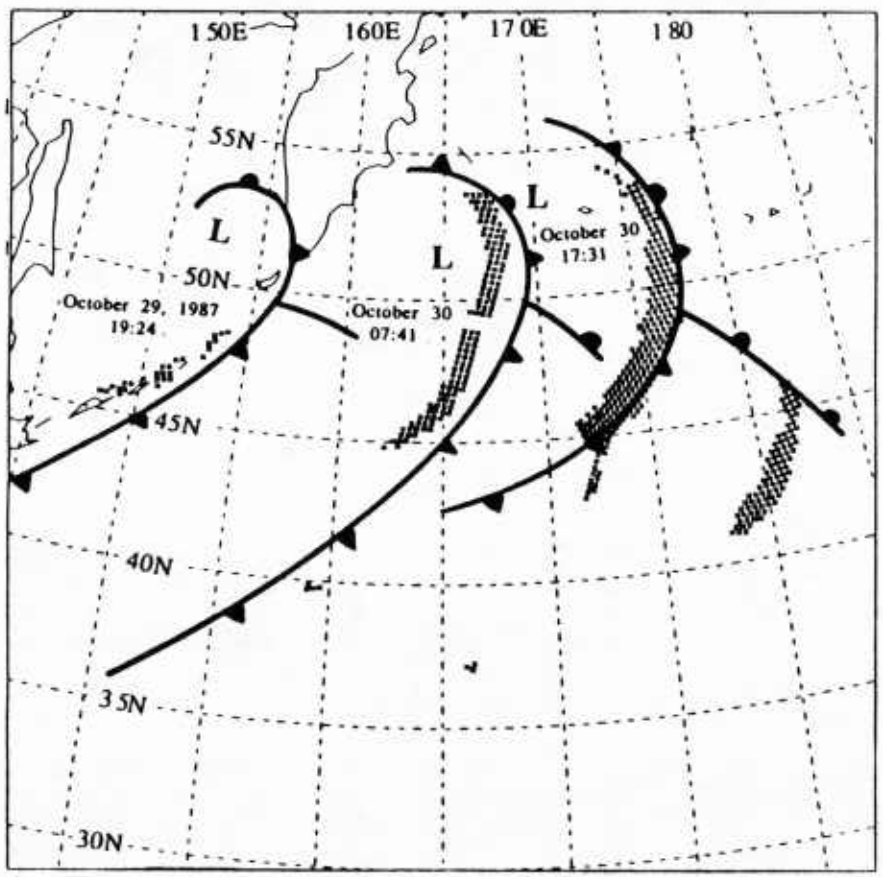

(d) Water vapor gradient flag '*' for all three orbits, plotted for threshold values of (.1 kg m^{-2})/km.

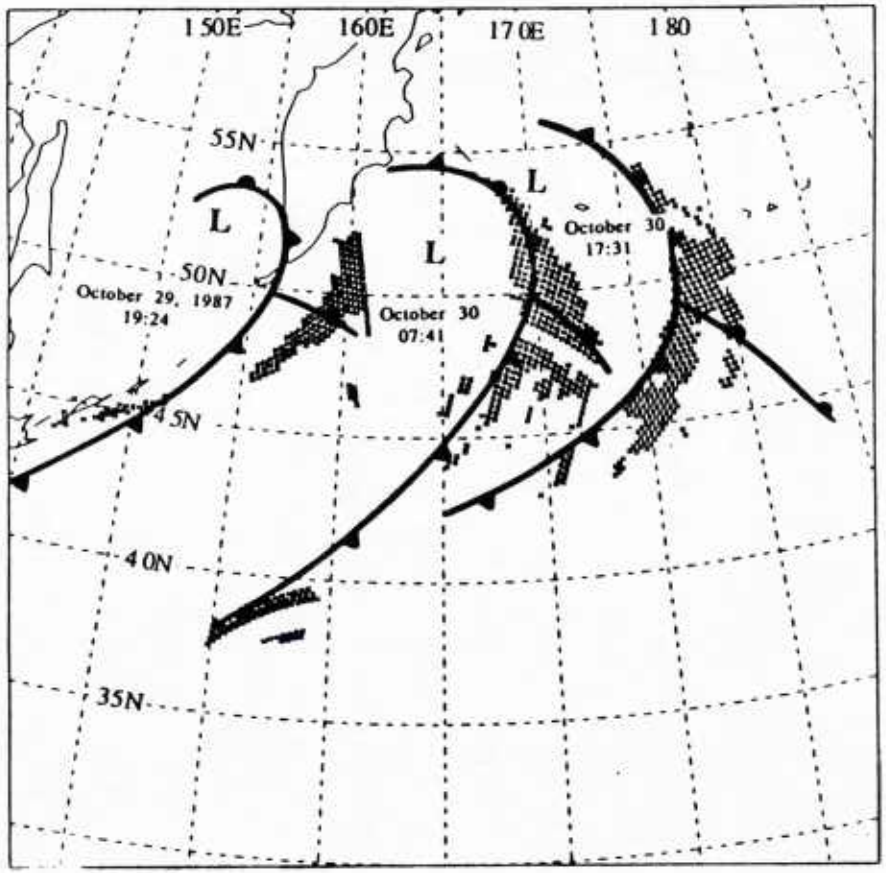

(e) Rain occurrence '*' for all three orbits, based on Tb_{37H} threshold of 200 K.

Figure 4(d)-(e). Occluded frontal systems crossing the Pacific Ocean, seen in DMSP F8 SSM/I data, October 29-30, 1987. The superimposed frontal analyses are from NMC synoptic surface maps with the positions linearly interpolated to the times of the three orbits. See text for discussion of discrepancies between flags and NMC analyses.

We must also keep in mind that the NMC frontal position has been interpolated to the time of the overpass by the satellite. The main point to be made is that IWV contours, WVG and rain flags give a special view of the position and shape of this frontal system. The third orbit at 17:31 UTC on October 30 shows perfect agreement between the NMC frontal analysis, the water vapor gradient and rain flags. However, an additional region of strong water vapor gradients is flagged at 180°E between 41° and 46°N. Such secondary regions of WVG flags were seen in SMMR data, but appear to be more common in SSM/I data. It may, therefore, be necessary to include a directional criterion with the WVG-flag, as suggested by Katsaros, et al. (1988a). Only regions whose gradient vector has an equatorward directed component of the proper sign would be used for flagging fronts (positive in the northern hemisphere, negative in the southern hemisphere). In this particular case, combination of the WVG and rain flags allows one to distinguish which of the two regions flagged by the WVG-flag locates the frontal system.

3.2 Case Studies from the North Atlantic Ocean

October 15, 1987, 19:16 UTC

This case is of special interest because it shows a low pressure center that was to deepen and become a dramatic storm over England on October 16. It was also not well forecast by the British Meteorological Office. In Figure 5 a swath over the region just west of Europe shows the appearance of a frontal system in several of the parameters derivable from SSM/I. The water vapor contour pattern (Figure 5a) shows strong gradients at the leading edge of a cold front (which even after advection of the NMC analysis to agree with the overpass time appears to be located about 1° longitude too far west). The water vapor and rain flags (Figures 5b and c) locate the cold front beautifully (after account has been taken of the slightly too slow advection) all the way from 33°N to the Bay of Biscay. In the North Sea, both the water vapor gradient flag and rain flag suggest that the frontal analysis is in error. The apex of the northernmost wave appears to be at 54°N, 0°E rather than 3° or

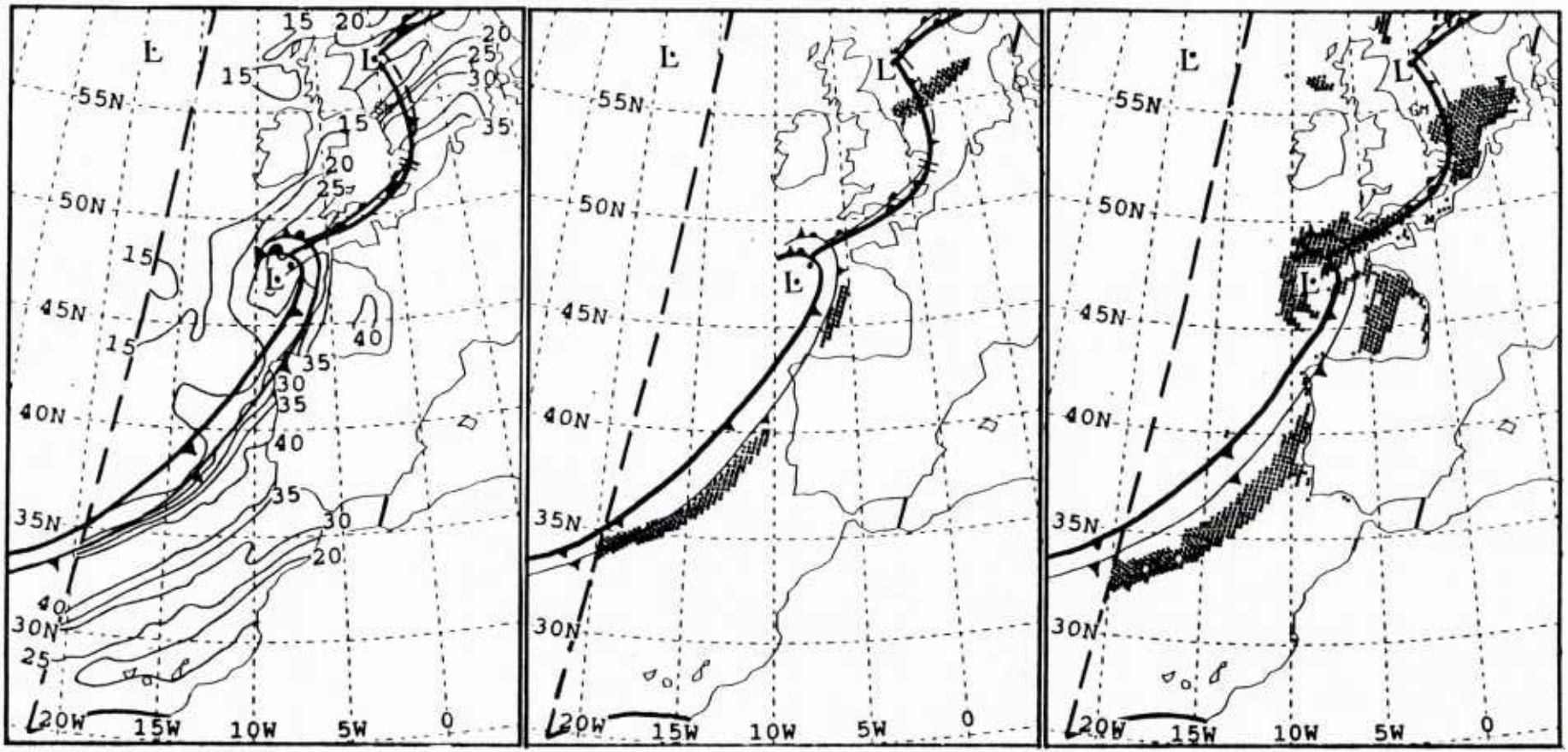

(a) Integrated water vapor in kg m^{-2}

(b) Water vapor gradient flag '*' plotted for threshold value of (0.1 kg m^{-2})/km

(c) Rain occurrence '*' based on T_{b37H} threshold of 200 K

Figure 5(a)-(c). Major cyclone affecting United Kingdom, DMSP F8 SSM/I, October 15, 1987 at 19:16 UTC, Orbit #1662. The thick superimposed frontal positions have been obtained from the NMC analysis at 18:00 UTC while the thin frontal positions represent the 19:00 UTC locations after advection of the 18:00 UTC NMC analysis positions. Note the disagreement between the NMC warm front and the water vapor gradient flag feature from 55° to 57°N and from 0° to 5°E. Figures 5d and 5e are on page 19.

4° farther north as indicated. According to Figure 5a, it appears that the warm front should be running SW to NE about 5° farther south than the NMC analysis indicates.

The 85 GHz scattering map seen in Figure 5d corroborates this interpretation, since it shows a region of strong signals associated with our estimated position of this wave, which is almost as large as the region associated with the mature cyclone south of England.

Figure 5e depicts SSM/I estimates of scalar wind speed associated with this storm. Since the cyclone was observed only a few hours before moving into Southern England and bringing with it a wind storm of record-breaking intensity, the performance of the Hughes wind speed algorithm in this case deserves particular attention.

In Figure 5(e), the ICLW estimates have been used to identify and blank out regions where the wind speed estimates are likely to be significantly contaminated by liquid water in the field of view. Obviously the winds in some of the most interesting regions of a storm are lost. Nevertheless, the picture that remains contains several interesting features. As one would expect, the wind speed increases towards the front, and is strongest in the Bay of Biscay, near the center of the low. Qualitatively, this pattern is entirely consistent with the detailed 18 UTC surface pressure analysis produced by the British Meteorological Office (not shown).

The maximum SSM/I wind estimates for this storm are in excess of 25 ms^{-1}. Given the 20 ms^{-1} sustained winds and gusts to 40 ms^{-1} that affected inland areas of England a short time later, the SSM/I values are quite plausible. Unfortunately, because we do not have ready access to ship reports of wind speed in that region, it has not yet been possible to directly corroborate the absolute magnitudes of the wind speed. Under more ordinary

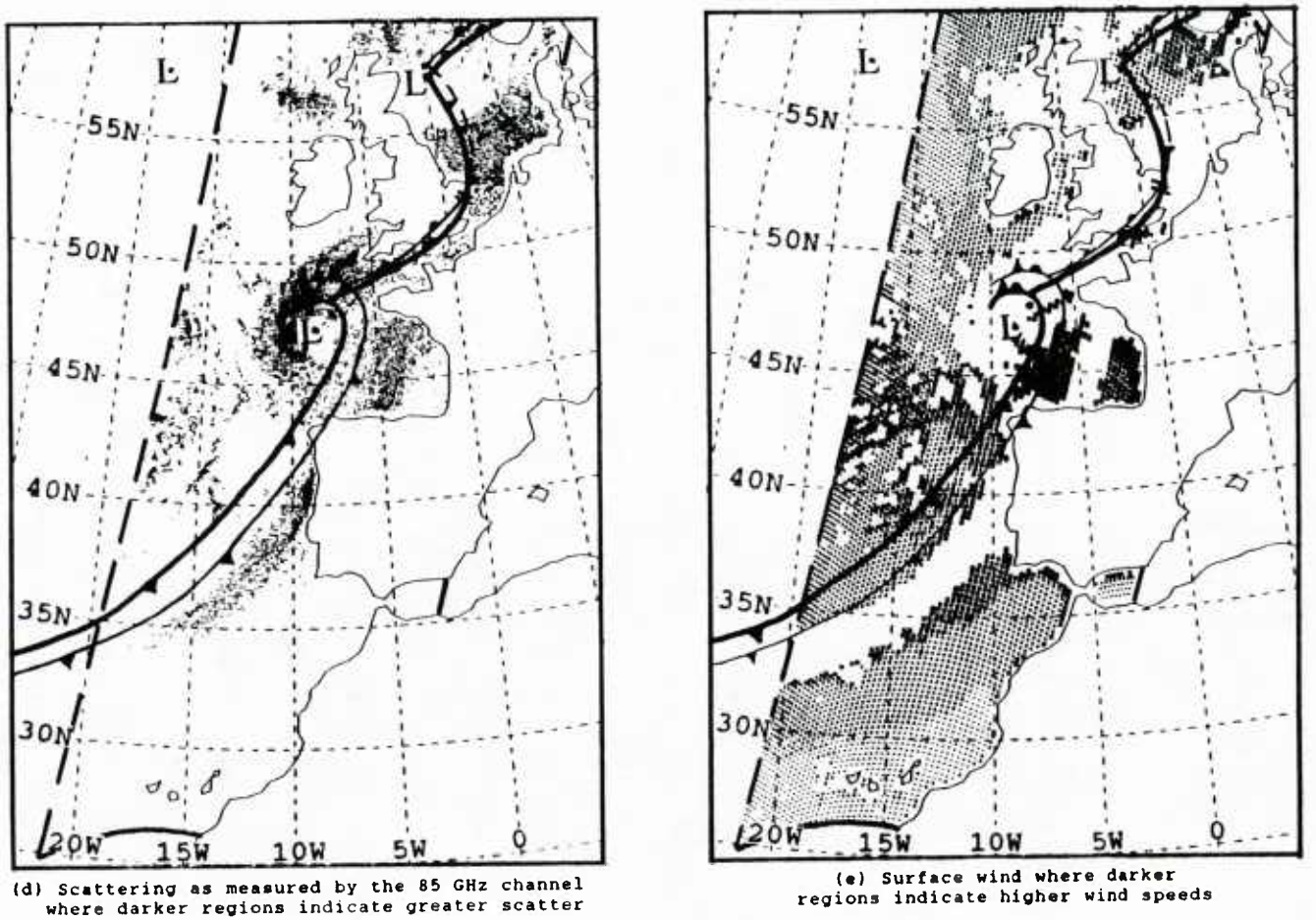

Figure 5(d)-(e). Major cyclone affecting United Kingdom, DMSP F8 SSM/I, October 15, 1987 at 19:16 UTC, Orbit #1662. The thick superimposed frontal positions have been obtained from the NMC analysis at 18:00 UTC while the thin frontal positions represent the 19:00 UTC locations after advection of the 18:00 UTC NMC analysis positions. In (e) data points have been omitted where the wind speed estimates would be severely contaminated by cloud liquid water in the field of view.

conditions, it has been our subjective impression that the Hughes algorithm tends to produce wind speeds which are biased high by about 5 ms^{-1}.

In the easternmost half of the Bay of Biscay, a sharp gradient in SSM/I wind speed appears, with the highest estimates appearing on the downwind side of the bay. The pressure analysis, however, shows a uniform gradient with straight isobars oriented SW-NE over the region, suggesting that the winds should be fairly constant. Because the wind speed algorithm actually responds directly to sea surface roughness and merely interprets the observed roughness in terms of wind speed, it may be surmised that the gradient is in fact a consequence of variations in the surface roughness due to factors other than wind speed alone. For example, the gradient in the SSM/I wind speed coincides approximately with the location of a marked decrease in the depth of the bay, so that the sensor may in fact be responding to the steepening and breaking of low-frequency gravity waves moving onto the coastal shelf. It could also be necessary to have an open-water fetch of order 100 km or more in order to fully develop that aspect of the surface roughness responsible for the signal sensed by the SSM/I. Since neither the interaction between wind and waves nor the response of microwave emission to surface roughness is well-understood, any such interpretation must be considered speculative.

Another region of large SSM/I wind speed estimates (15-20 ms^{-1}) appears behind the cold front, in the vicinity of 43N, 15W. The highest speeds appear in close association with a pattern of deep convection within the cold air mass, as indicated by the appearance of blanked out clusters of pixels resulting from the ICLW screening. The presence of the deep clouds raises questions about the reality of the SSM/I winds in this area. On the one hand, it is possible that the more intense convective instability behind the front is indeed associated with the strongest surface winds in the cold air mass, due to more efficient momentum exchange through the boundary layer or for any of a number of other reasons.

On the other hand, there is the ever present spectre of rain contamination of the wind signal by convective elements too small to detect and screen out with only the low resolution channels of the SSM/I.

October 16, 1987

This case shows our, by-now-classic appearance in the integrated water vapor pattern (Figure 6a) of a cold front between 31° and 37°N. It is flagged by the WVG and rain flag and appears in the 85 GHz scattering map (Figures 6d). A new cold front at 10-15°W, 40-47°N does not have a signal in the water vapor field, the WVG flag, or the rain flag. Interestingly, however, the 85 GHz scattering map (Figure 6d) shows activity at this cold front and west of it, with another strong activity center at 50°N. The NMC surface analysis shows only a weak pressure gradient with no trough or developing depression; so, we attribute these signals to convective clouds. The wind speed map for this case (Figure 6e) shows strong winds, 15-20 ms^{-1}, in the whole region where the 85 GHz scattering indicates deep convection and, additionally, south and west of the tail and at the northerly cold front at 40°N, 15°W.

October 17, 1987

An occluded front is seen between 45° and 50°N at about 23°W. This front has only weak water vapor gradients associated with it (Figure 7a), and no WVG-flags occur for a threshold of 0.1 kg m^{-2}/km. The rain flags, shown in Figure 7b, do not outline this front either, but a broad region of distributed precipitation is flagged a substantial distance to the east of this occluded front. The 85 GHz map, Figure 7c, and the liquid water map, Figure 7d, both show this broad region of hydrometeors from 45° to 53°N and from 10° to 20°W. The 85 GHz pattern is particularly interesting, showing regions of intense scattering, which appear to line up in a band stretching from 43°N, 23°W to 50°N, 17°W. The associated weather map, Figure 7e, shows no special features except a weak trough in the general

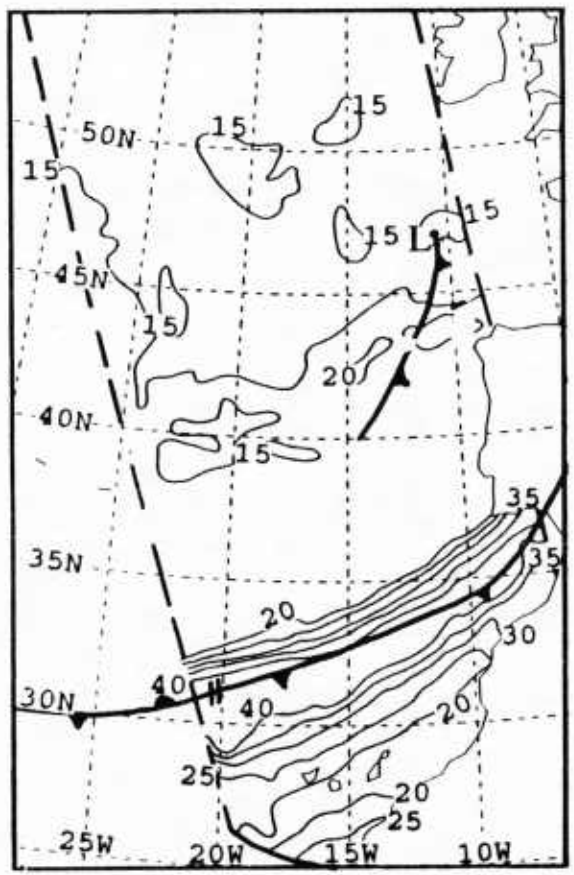

(a) Integrated water vapor in kg m^{-2}

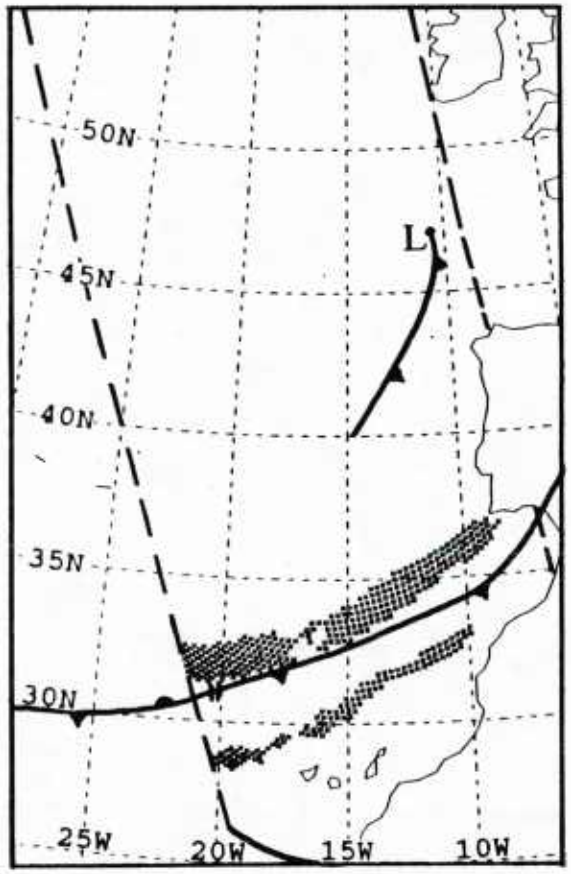

(b) Water vapor gradient flag '*' plotted for threshold value of (0.1 kg m^{-2})/km

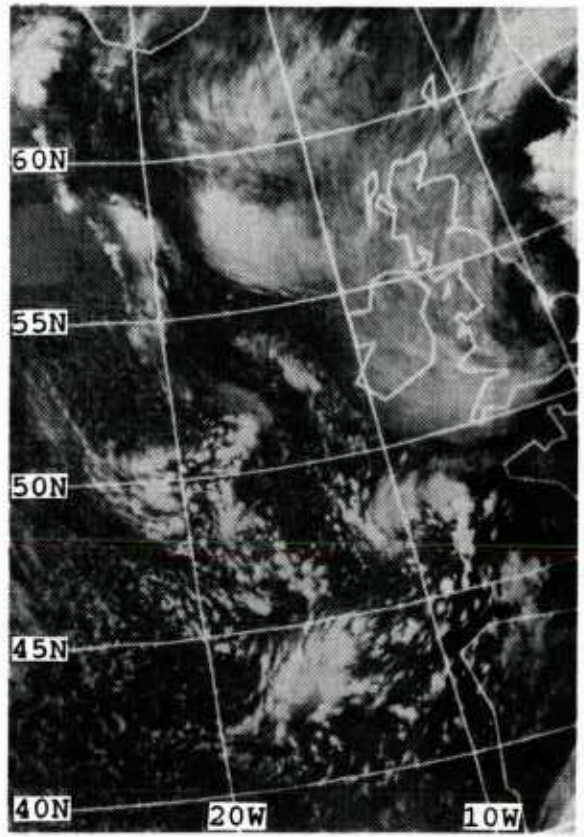

(c) NOAA-9 infrared satellite image of the North Atlantic Ocean for October 16, 04:42 UTC.

Figure 6(a)-(c). Tail of cold front, DMSP F8 SSM/I, October 16, 1987 at 06:45 UTC, Orbit #1669. In (a) and (b) the superimposed frontal positions have been obtained from the NMC analysis at 06:00 UTC. Note that the cold front from 40° to 47°N and from 11° to 14°W is not apparent in most of the fields. Figure 6c is an image produced by the Department of Electrical Engineering at the University of Dundee. Figures 6d and 6e are on the following page.

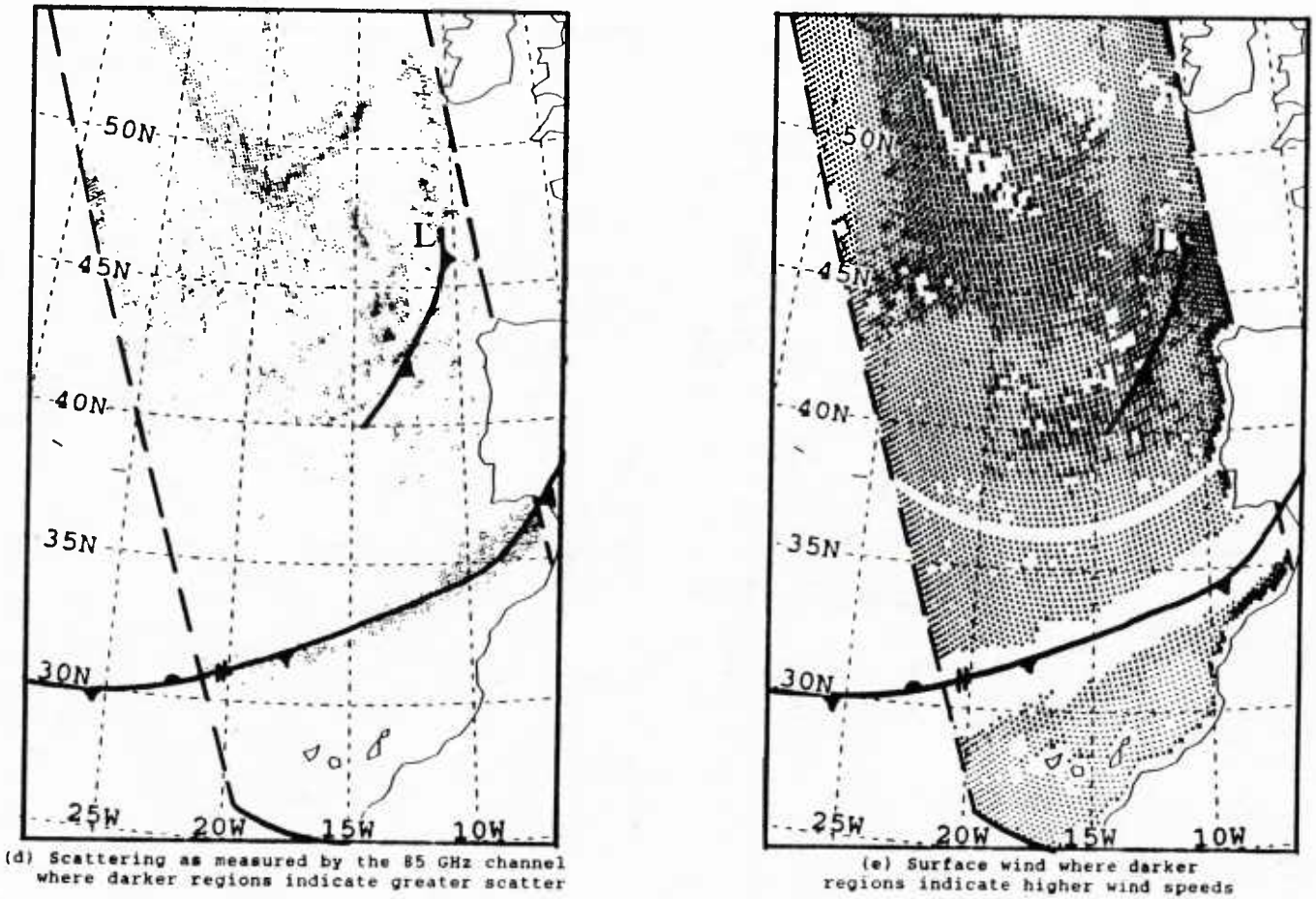

Figure 6(d)-(e). Tail of cold front, DMSP F8 SSM/I, October 16, 1987 at 06:45 UTC, Orbit #1669. In (d) and (e) the superimposed frontal positions have been obtained from the NMC analysis at 06:00 UTC. In (e) data points have been omitted where the wind speed estimates would be severely contaminated by cloud liquid water in the field of view.

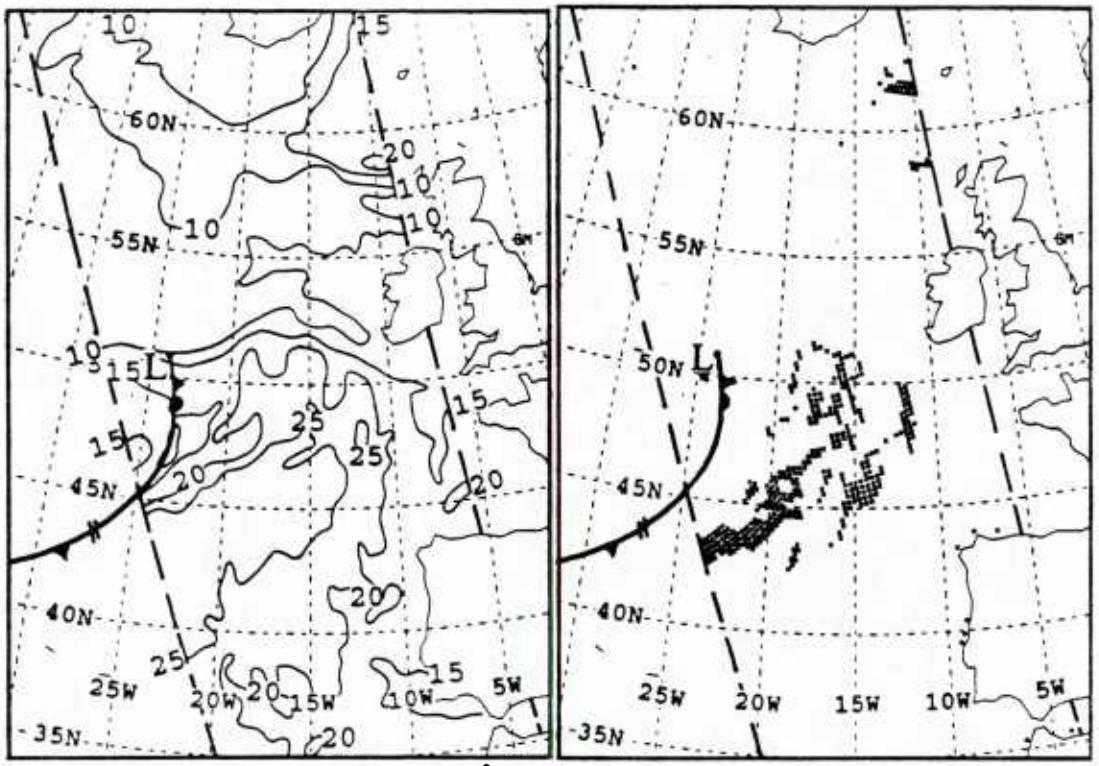

(a) Integrated water vapor in kg m^{-2}

(b) Rain occurrence '*' based on T_{b37H} threshold of 200 K

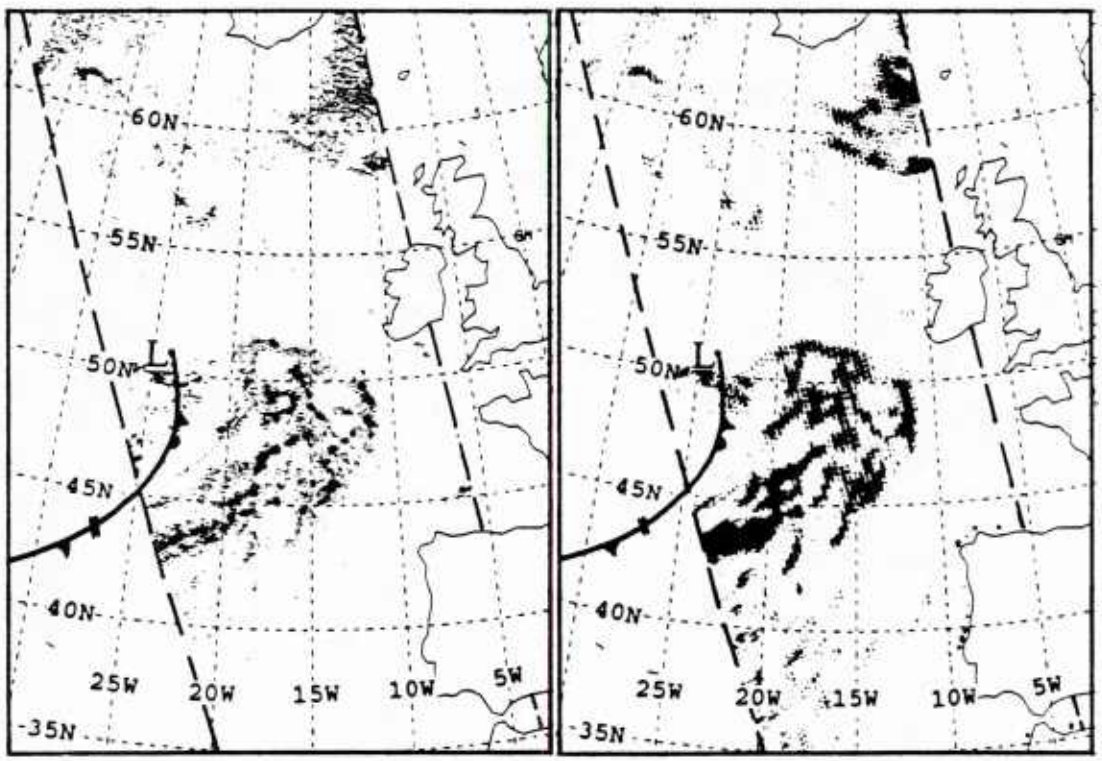

(c) Scattering as measured by the 85 GHz channel where darker regions indicate greater scatter

(d) Integrated cloud liquid water where darker regions indicate larger values

Figure 7(a)-(d). Convective region ahead of frontal system, DMSP F8 SSM/I, October 17, 1987 at 06:35 UTC, Orbit #1683. In (a)-(d) the superimposed frontal positions have been obtained from the NMC analysis at 06:00 UTC. Figures 7e and 7f are on the following page.

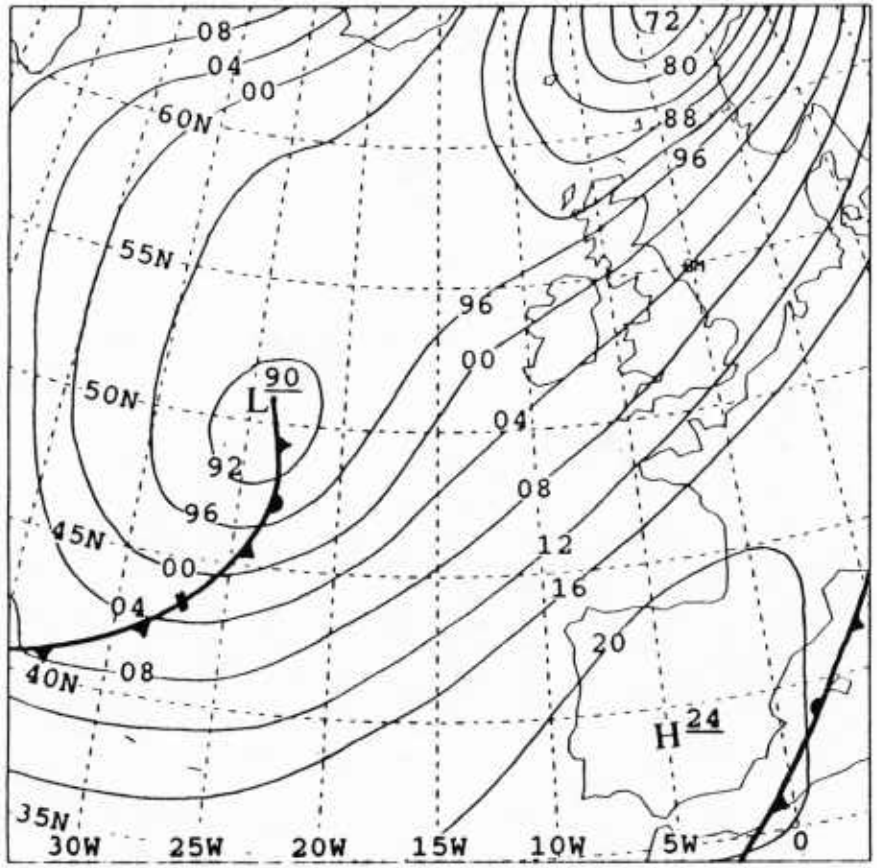

(e) NMC surface analysis for October 17, 1987, 06:00 UTC.

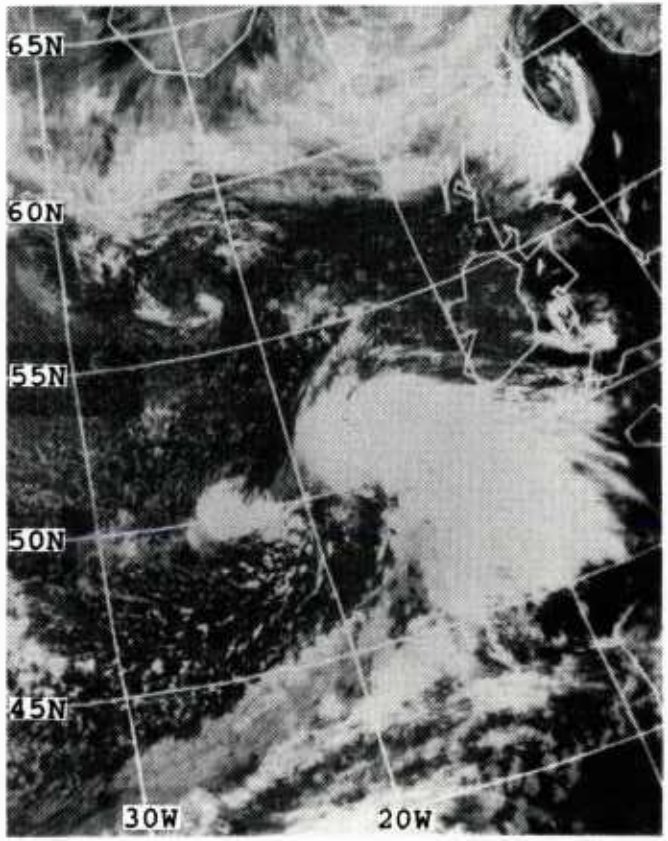

(f) NOAA-10 infrared satellite image of the North Atlantic Ocean for October 17, 09:38 UTC.

Figure 7(e)-(f). Frontal system with convective region to the east. The front located from 41° to 51°N and from 23° to 35°W on the weather map, in (e), is identical to the front superimposed on (a)-(d). Figure 7f is an image produced by the Department of Electrical Engineering at the University of Dundee.

vicinity, but the closest satellite image in time, Figure 7f, obtained several hours later shows a large cloud mass east of 20°W. Further investigation is required to ascertain whether the SSM/I data were harbingers of rapid development of the trough.

October 18, 1987

Figure 8a shows the water vapor pattern associated with this frontal system. A typical post-frontal gradient is seen, and readily caught by the WVG-flag at the tail position (Figure 8b). Closer to England the threshold appears to have been too large to locate the front, however. The rain flag, Figure 8c, gives no doubt where this front may be found, and the 85 GHz pattern outlines not only the cold front, but also the occlusion, giving a strong hint that, if the occlusion is associated with a spiral cloud band, NMC has drawn it in the wrong place (Figure 8d).

The surface wind speed associated with this case shows maximum winds of 15 to 20 ms^{-1} west of Ireland; these speeds are supported by the NMC surface map that shows a station with a wind speed of 17 ms^{-1} at 54°N, 15°W (Figure 8e). The 85 GHz pattern shows activity only in the northerly portion of this region, so we don't expect much contamination of the wind speed estimates. The same may be true in the Bay of Biscay. The high wind speeds and 85 GHz scattering just south of Iceland are associated with the cold front of an old system that shows no strong gradients in the IWV pattern, nor does NMC draw a front in that region of the SSM/I swath. Whether 15-20 ms^{-1} winds occurred south of Iceland at this time cannot be readily verified. The NMC surface pressure analysis for 06:00 UTC shows a weak pressure gradient in that region; to the north and to the south the pressure gradient is about twice as strong. It appears that the SSM/I wind speeds could have improved the surface pressure analysis in this case.

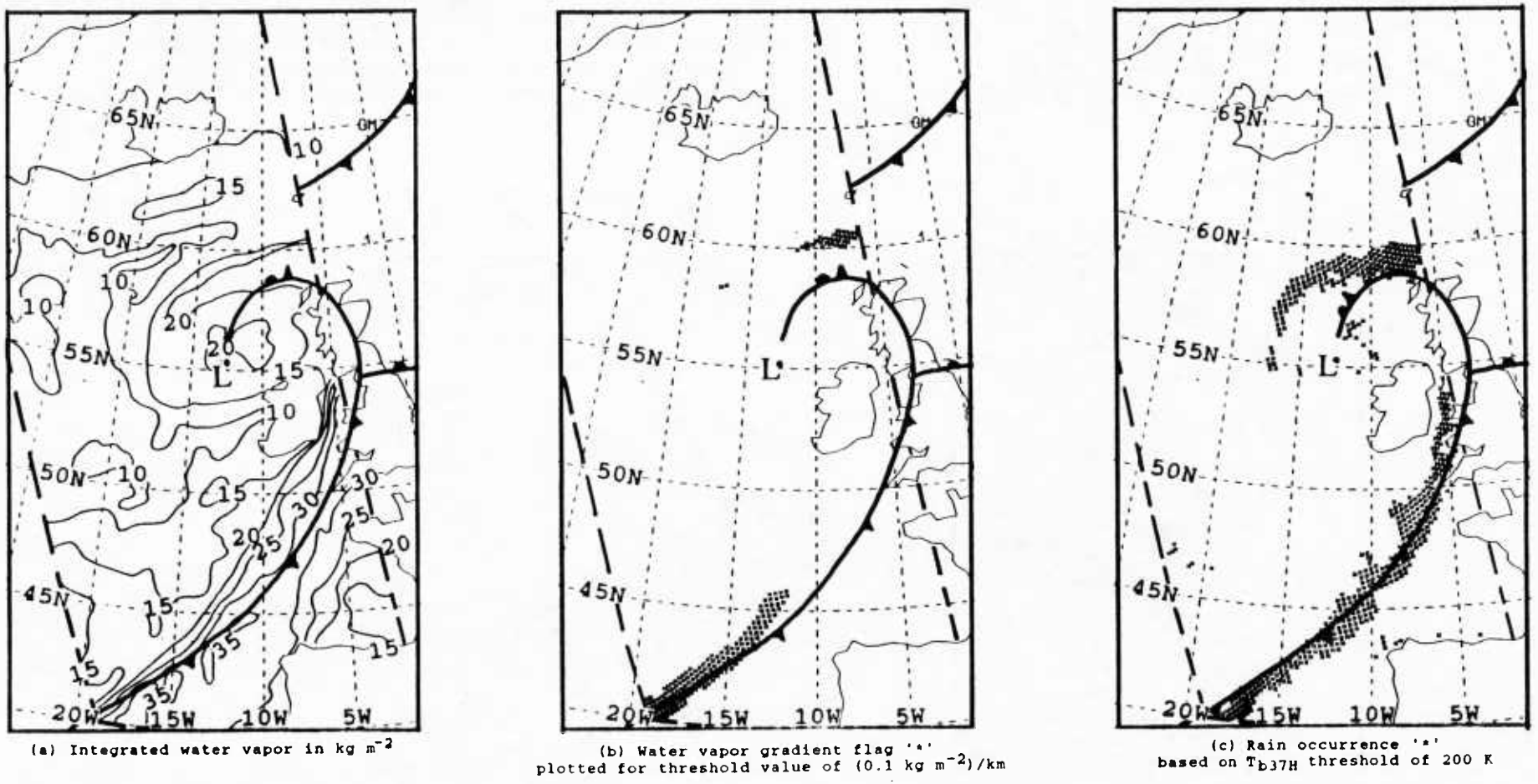

Figure 8(a)-(c). Occluded cyclone, DMSP F8 SSM/I, October 18, 1987 at 06:24 UTC, Orbit #1697. The superimposed frontal positions have been obtained from the NMC analysis at 06:00 UTC. Note that the gradient in (a) from 53° to 55°N and from 6° to 7°W is an artificial feature caused by land contamination in the received signal. Figures 8d and 8e are on the following page.

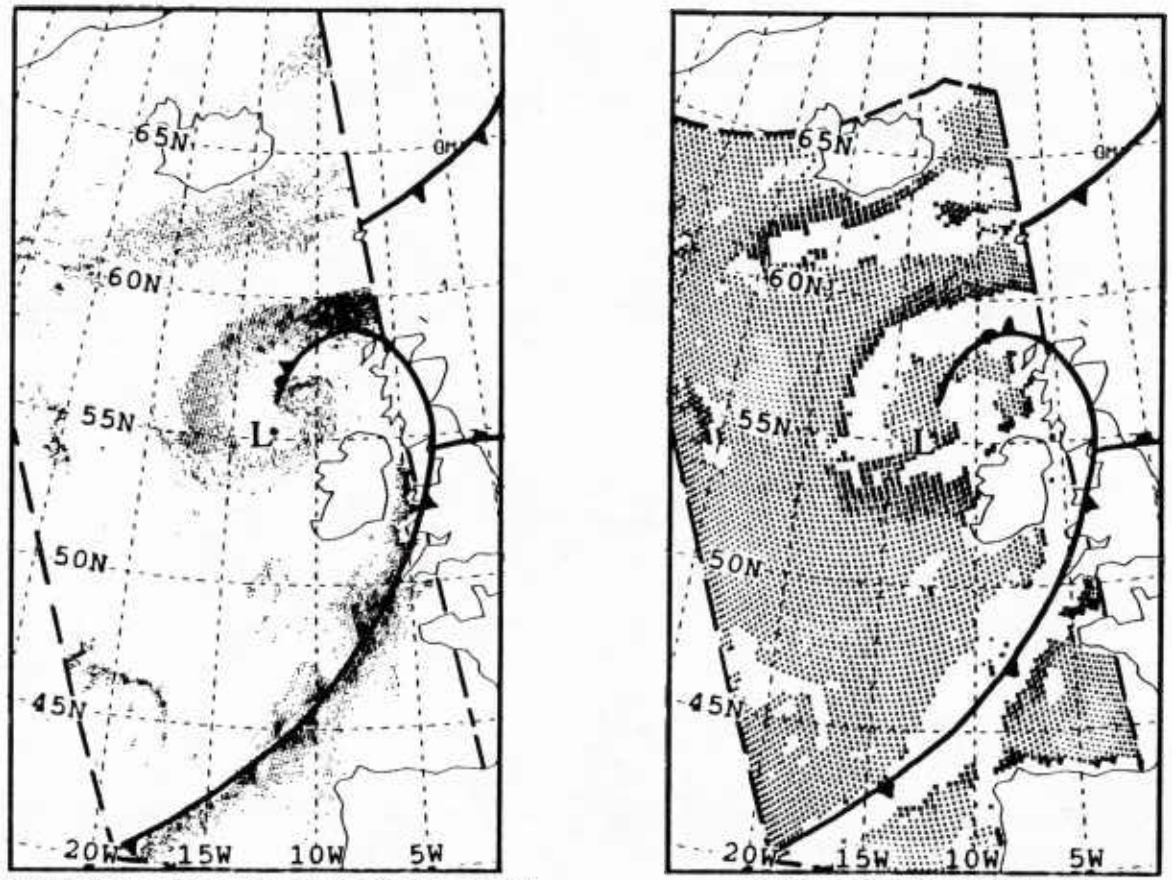

Figure 8(d)-(e). Occluded cyclone, DMSP F8 SSM/I, October 18, 1987 at 06:24 UTC, Orbit #1697. The superimposed frontal positions have been obtained from the NMC analysis at 06:00 UTC. In (e) data points have been omitted where the wind speed estimates would be severely contaminated by cloud liquid water in the field of view.

October 19, 1987

Twenty-four hours after the previous case this occluded frontal system still shows a sharp gradient west and south of England (Figure 9a). The WVG-flag outlines this front (Figure 9b), as does Integrated Cloud Liquid Water (Figure 9c). The interesting feature of this case is the appearance of enlarged regions of integrated cloud liquid water, where a wave is apparently developing along the cold front at 47° N, 8°W, and where a new low with an associated trough is analyzed at 50°N, 14°W. A second feature of interest is the support of the analyzed "trof" at 45°N, 12°W by a relative maximum region of $\geq$ 20 kg m^{-2} in the water vapor field (Figure 9a).

4. DISCUSSION

Our impression from the cases studied using SSM/I data is that this new instrument performs very well, indeed. The wider swath, twice that of the SMMR, and the continuous operation (compared to every other day for SMMR) insures that the SSM/I data will provide a tremendous improvement over the SMMR data for studying midlatitude cyclones over the sea. We do not observe any obvious large errors in the SSM/I data analyzed with the Hughes algorithm, but we have not attempted a validation effort, since that is being carried out expertly elsewhere (Hollinger, 1988, personal communication). The view that SSM/I presents of midlatitude cyclones is unique and detailed. Mesoscale features such as frontal waves and rain bands, dry slots and convective activity are readily recognized in the IWV, ICLW, rain occurrence and 85 GHz scattering patterns, and their location and areal extent can be ascertained. These features could undoubtedly be used to advantage by forecasters in improving short range forecasts, if they were available in near real time. At present, they can be used for research on midlatitude cyclonic storms.

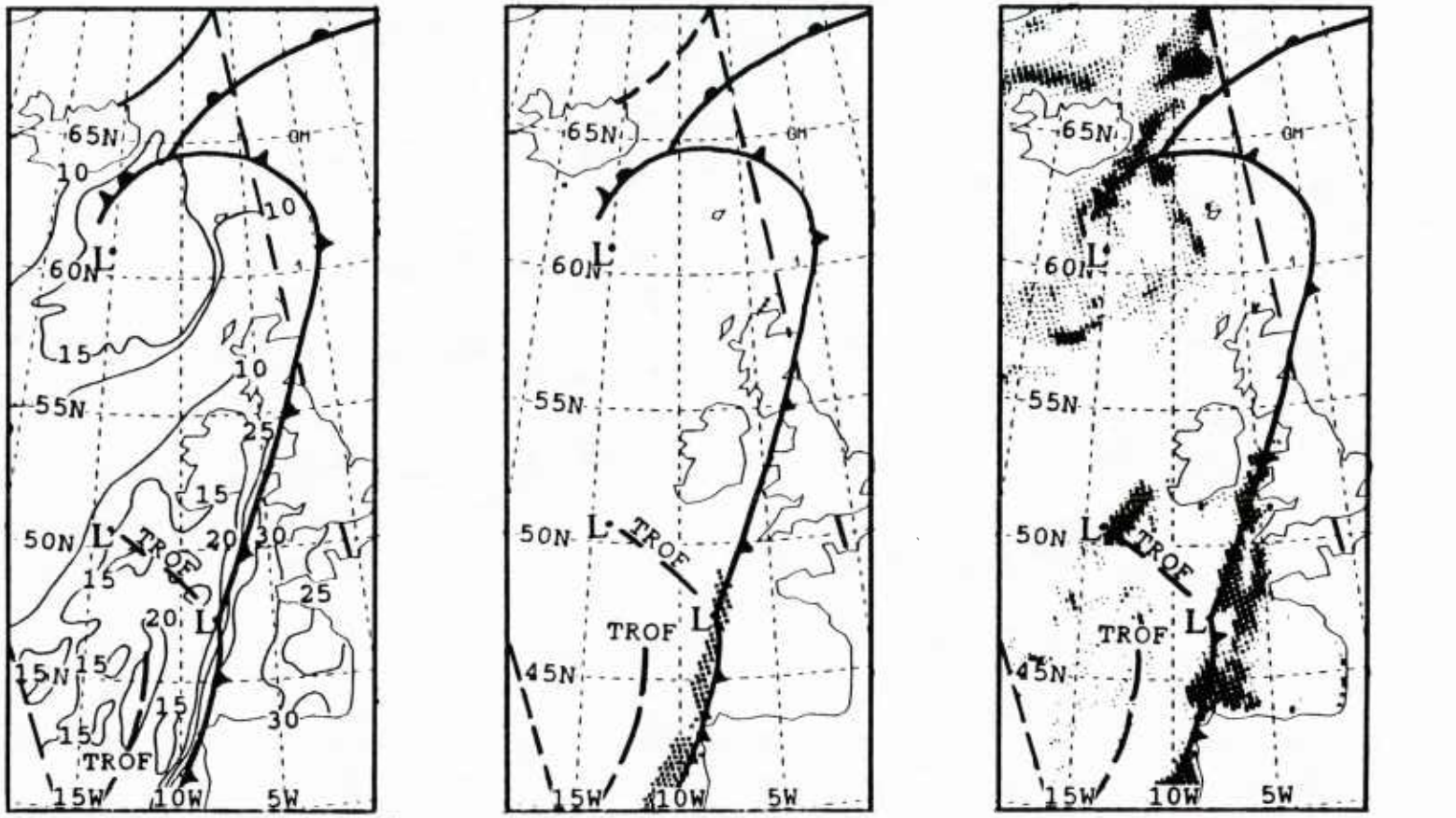

Figure 9(a)-(c). Old occluded cyclone with developing wave, DMSP F8 SSM/I, October 19, 1987 at 06:11 UTC, Orbit #1711. In (a)-(c) the superimposed frontal and "trof" positions have been obtained from the NMC analysis at 06:00 UTC. Note that the "trof" from 40° to 47°N and from 10° to 15°W is marked by a region of relatively high water vapor content in 9a.

That the threshold value for flagging fronts is larger for the SSM/I data than for our SMMR data is at first surprising, since the information is in terms of geophysical units, and the magnitudes of the water vapor should be invariant with the sensor. We have found that the IWV gives a strong and robust signal. However, the data sampling and processing for each sensor is handled differently. The brightness temperature channels used for water vapor estimates from the SMMR were first regridded onto a rectangular array with grid spacing of 60 km; the SSM/I data, on the other hand, are used directly at their original sampling density of one pixel every 25 km. The regridding of the SMMR data entails spatial averaging which leads to some degradation of the resolution. Thus, although the nominal spatial resolution of the water vapor sensitive channels on each sensor is similar -- about 50 km, the effective resolution is poorer for the SMMR (no better than 60 km). In addition, SSM/I gradient values are calculated from pairs of points which are separated by a much smaller distance. As a consequence of both of these facts, a very sharp gradient of limited spatial extent is more faithfully reproduced in the SSM/I data than in the SMMR data. This might normally be interpreted as giving an advantage to the SSM/I, but the undesirable result is that small but sharp variations in the water vapor field which have nothing to do with fronts are flagged by the SSM/I, when they would be ignored by the SMMR. Simply increasing the threshold used to flag fronts cannot completely alleviate the problem. Possible remedies include smoothing the SSM/I field with a larger window before calculating the gradient and/or calculating the gradient between more distant pairs of points. We are still experimenting with all of these options to find a procedure which most effectively and reliably locates fronts without raising an undue number of false alarms.

As discussed earlier, the water vapor gradient flagging routine for locating fronts occasionally identifies large water vapor gradients at locations other than in the immediate vicinity of a front. Thus, when the present form of the algorithm is used in isolation, there is some chance that a front may be diagnosed where no front is actually present. In most

cases, the greatest potential for this kind of error appears to occur 100-1000 km ahead of a cold front, where the very moist air mass on the warm side of the front may form a relatively sharp boundary with the dry air associated with the neighboring high pressure region farther downstream. An example of such a case was seen in Figure 1.

On average, the value of the WVG appears to be somewhat lower at such a boundary than along a true front, but sometimes, the WVG values found in such cases may exceed those found in a true front having only weak gradients. Thus, although increasing the WVG threshold might help to reduce the number of false alarms, it would also reduce the number of correctly identified fronts.

When the SSM/I WVG flags are plotted, the above-described "false alarm" condition usually appears as a narrow secondary line of flags roughly parallel to and ahead of the legitimate cold front. Such a double row of flags should always be considered suspect, unless there is other evidence supporting the presence of two cold fronts in close proximity to each other. An example of such evidence is the rain flag. Quite often, rain will be prominent along and just ahead of the true front, but it will seldom appear near a false front identified by the WVG flags.

To help alleviate the problem of false-positive diagnoses in a semi-automated environment, a more sophisticated WVG flagging algorithm can be envisioned in which directional information is exploited. Typically, the water vapor gradient vector (i.e., the direction along which the IWV increases most rapidly) is oriented approximately perpendicular to the front and directed toward the warm sector of the cyclone. For example, if a cold front in the Northern Hemisphere is oriented northeast-southwest (a very common case), the WVG vector is directed approximately southeast. On the other hand, most of the "false fronts" that we have seen flagged by the WVG routine have been associated with larger IWV

values poleward and westward of the WVG flags. Very few true fronts appear to exhibit this orientation. Thus, it seems probable that, by excluding from consideration water vapor gradients having both a westward and poleward component, the number of false-positives may be drastically reduced without greatly reducing the number of correctly flagged fronts.

The actual implementation of such an algorithm is straightforward. Indeed, the calculation of the orthogonal vector gradient components of the IWV field (relative to the axis of the satellite swath) is already performed as an intermediate step in calculating the scalar WVG. By keeping the cross-swath and along-swath gradient components and then rotating these into the geographic coordinate system, a scalar WVG exceeding the threshold can be further screened for poleward- and westward-directed components. If both are present, that flag would be discarded.

When advocating the practical use of SSM/I WVG-flags and precipitation flags for locating fronts, we don't mean to imply that with typical operational data available, an experienced forecaster could not usually have located the front as well. The particular value of the WVG-flag, we surmise, is that it is totally objective (once a threshold has been established) and it can be readily made available with very little sophistication in computer support.

Integrated cloud liquid water, ICLW, and 85 GHz scattering by large ice particles are two parameters that show promise for diagnosing developing waves, intense convection and storm intensity. When identifying cloud and rain features it is likely that the resolution of a particular satellite sensor must be carefully considered. In context of measuring cloudiness and rain from space, Gabriel, et al. (1988) discuss the dependence of critical measures of a radiation field on the resolution of the remote sensors and suggest that resolution-independent models in terms of "continuous multifractals" allow later development of

optimal sampling, averaging and calibration procedures. These are interesting concepts to pursue, but beyond the scope of this research.

The wind speed calculated with the Hughes algorithm shows features that appear to be realistic by comparison with weather maps. However, once the regions of the swath have been eliminated, where rain contaminates the wind speed algorithm, most of the interesting parts of weather systems have been lost for wind speed determination. However, cols and high pressure regions, and regions of high wind speed away from fronts, can often be quite well defined with the surface wind determination. This feature may be very helpful for surface pressure field analysis over remote oceanic regions, and could thereby become valuable for weather forecasting, even though these regions do not themselves represent dangerous or dramatic weather conditions.

5. ACKNOWLEDGEMENTS

We are grateful to Frank J. Wentz and Erica Francis for providing us the SSM/I tapes, to Kay Dewar for drafting the weather map figures and to Janet Meadows, who typed the manuscript with great care. We appreciate the continuous encouragement by Drs. Andreas Goroch and Paul Tag at the Naval Environmental Prediction Research Facility throughout this work.

6. REFERENCES

Gabriel, P., S. Lovejoy, G.L. Austin and D. Schertzer, 1988: Multifractal analysis of resolution dependence in satellite imagery. *Geophys. Res. Let.*, **15**, 1373-1376.

Hollinger, J., R. Lo, G. Poe, R. Savage and J. Pierce, 1987: *Special Sensor Microwave/Imager User's Guide*. Naval Research Laboratory, Washington, D.C., 177 pp.

Katsaros, K.B., G.W. Petty and U. Hammarstrand, 1988a: Liquid Water and Water Vapor in Mid-Latitude Cyclones Observed by Microwave Radiometry and Compared to Model Calculations. *Proceedings of Palmen Memorial Symposium,* Aug. 29-Sept. 2, 1988, Helsinki, Finland, one page.

Katsaros, K.B., I.A. Bhatti, L.A. McMurdie and G.W. Petty, 1988b: Passive Microwave Measurements of Water Vapor Fields and Rain for Locating Fronts in Cyclonic Storms. Contract Report CR 88-01, March 1988. Naval Environmental Prediction Research Facility, Monterey, CA, 93943-5006, 45 pp.

Spencer, R.W., 1986: A satellite passive 37 GHz scattering-based method for measuring oceanic rain rates. *J. Clim. Appl. Meteor.*, **25**, 754-766.

Wentz, F.J., L.A. Mattox and S. Peteherych, 1986: New algorithms for microwave measurements of ocean winds: applications to Seasat and the Special Sensor Microwave/Imager. *J. Geophys. Res.*, **91**, 2289-2307.

Distribution

ASST. FOR ENV. SCIENCES
ASST. SEC. OF THE NAVY (R&D)
ROOM 5E731, THE PENTAGON
WASHINGTON, DC 20350

CHIEF OF NAVAL RESEARCH
LIBRARY, CODE 01232L
BALLSTON TOWER #1
800 QUINCY ST.
ARLINGTON, VA 22217-5000

OFFICE OF NAVAL RESEARCH
CODE 1122AT, ATMOS. SCIENCES
ARLINGTON, VA 22217-5000

OFFICE OF NAVAL RESEARCH
ENV. SCI. PROGRAM, CODE 112
ARLINGTON, VA 22217-5000

OFFICE OF NAVAL RESEARCH
ATTN: HEAD, OCEAN SCIENCES DIV
CODE 1122
ARLINGTON, VA 22217-5000

OFFICE OF NAVAL RESEARCH
CODE 1122 MM, MARINE METEO.
ARLINGTON, VA 22217-5000

OFFICE OF NAVAL TECHNOLOGY
ONR (CODE 22)
800 N. QUINCY ST.
ARLINGTON, VA 22217-5000

CHIEF OF NAVAL OPERATIONS
OP-962
U.S. NAVAL OBSERVATORY
WASHINGTON, DC 20390

LIBRARY
NAVAL ARCTIC RESEARCH LAB
BARROW, AK 99723

COMMANDING OFFICER
NAVAL RESEARCH LAB
ATTN: LIBRARY, CODE 2620
WASHINGTON, DC 20390

COMMANDING OFFICER
NORDA, CODE 335
JCSSC, MS 39529-5004

COMMANDER
NAVAL OCEANOGRAPHY COMMAND
JCSSC, MS 39529

COMNAVOCEANCOM
ATTN: CODE N5
J.C. STENNIS SPACE CENTER
JCSSC, MS 39529-5000

COMMANDING OFFICER
NAVAL OCEANOGRAPHIC OFFICE
BAY ST. LOUIS
JCSSC, MS 39522-5001

COMMANDING OFFICER
FLENUMOCEANCEN
MONTEREY, CA 93943-5005

SUPERINTENDENT
LIBRARY REPORTS
U.S. NAVAL ACADEMY
ANNAPOLIS, MD 21402

DIRECTOR OF RESEARCH
U.S. NAVAL ACADEMY
ANNAPOLIS, MD 21402

NAVAL POSTGRADUATE SCHOOL
METEOROLOGY DEPT.
MONTEREY, CA 93943-5000

LIBRARY
NAVAL POSTGRADUATE SCHOOL
MONTEREY, CA 93943-5002

COMMANDER
NAVAIRSYSCOM, CODE 526W
WASHINGTON, DC 20361-0001

COMMANDER, SPAWARSYSCOM
ATTN: CODE PMW-141
NAT. CTR. #1
WASHINGTON, DC 20363-5100

COMMANDER
PACMISTESTCEN
GEOPHYSICS OFFICER
PT. MUGU, CA 93042

USAFETAC/TS
SCOTT AFB, IL 62225

3350TH TECH. TRNG GROUP
TTGU/2/STOP 623
CHANUTE AFB, IL 61868

AFGWC/DAPL
OFFUTT AFB, NE 68113

AFGL/LY
HANSCOM AFB, MA 01731

COMMANDER/DIRECTOR
ATMOS. SCI. LABORATORY
ATTN: SLCAS-AE-A (HANSEN)
WHITE SANDS MR, NM 88002-5501

DIRECTOR (6)
DEFENSE TECH. INFORMATION
CENTER, CAMERON STATION
ALEXANDRIA, VA 22314

CHIEF
MARINE & EARTH SCI. LIBRARY
NOAA, DEPT. OF COMMERCE
ROCKVILLE, MD 20852

DIRECTOR
NATIONAL HURRICANE CENTER
NOAA, GABLES ONE TOWER
1320 S. DIXIE HWY
CORAL GABLES, FL 33146

NATIONAL WEATHER SERVICE
WORLD WEATHER BLDG., RM 307
5200 AUTH ROAD
CAMP SPRINGS, MD 20023

DIRECTOR
GEOPHYS. FLUID DYNAMICS LAB
NOAA, PRINCETON UNIVERSITY
P.O. BOX 308
PRINCETON, NJ 08540

DIRECTOR
TECHNIQUES DEVELOPMENT LAB
GRAMAX BLDG.
8060 13TH ST.
SILVER SPRING, MD 20910

DIRECTOR
NATIONAL WEATHER SERVICE
GRAMAX BLDG.
8060 13TH ST.
SILVER SPRING, MD 20910

HEAD, ATMOS. SCIENCES DIV.
NATIONAL SCIENCE FOUNDATION
1800 G STREET, NW
WASHINGTON, DC 20550

ATMOSPHERIC SCIENCES DEPT.
UCLA
405 HILGARD AVE.
LOS ANGELES, CA 90024

CHAIRMAN, METEOROLOGY DEPT.
CALIFORNIA STATE UNIVERSITY
SAN JOSE, CA 95192

UNIVERSITY OF WASHINGTON
ATMOSPHERIC SCIENCES DEPT.
SEATTLE, WA 98195

CHAIRMAN, METEOROLOGY DEPT.
PENNSYLVANIA STATE UNIV.
503 DEIKE BLDG.
UNIVERSITY PARK, PA 16802

UNIVERSITY OF HAWAII
METEOROLOGY DEPT.
2525 CORREA ROAD
HONOLULU, HI 96822

AMERICAN METEORO. SOCIETY
METEOR. & GEOASTRO. ABSTRACTS
P.O. BOX 1736
WASHINGTON, DC 20013

DIRECTOR, JTWC
BOX 17
FPO SAN FRANCISCO 96630

BUREAU OF METEOROLOGY
BOX 1289K, GPO
MELBOURNE, VIC, 3001
AUSTRALIA

EUROPEAN CENTRE FOR MEDIUM
RANGE WEATHER FORECASTS
SHINFIELD PARK, READING
BERKSHIRE RG29AX, ENGLAND